ORIGINAL RESEARCH PAPER

Impact of rough stochastic volatility models on long-term life insurance pricing

Jean-Loup Dupret[1] · **Jérôme Barbarin[1]** · **Donatien Hainaut[1]**

Abstract

The Rough Fractional Stochastic Volatility (RFSV) model of Gatheral et al. (Quant Financ 18(6):933–949, 2014) is remarkably consistent with financial time series of past volatility data as well as with the observed implied volatility surface. Two tractable implementations are derived from the RFSV with the rBergomi model of Bayer et al. (Quant Financ 16(6):887–904, 2016) and the rough Heston model of El Euch et al. (Risk 84–89, 2019). We now show practically how to expand these two rough volatility models at larger time scales, we analyze their implications for the pricing of long-term life insurance contracts and we explain why they provide a more accurate fair value of such long-term contacts. In particular, we highlight and study the long-term properties of these two rough volatility models and compare them with standard stochastic volatility models such as the Heston and Bates models. For the rough Heston, we manage to build a highly consistent calibration and pricing methodology based on a stable regime for the volatility at large maturity. This ensures a reasonable behavior of the model in the long run. Concerning the rBergomi, we show that this model does not exhibit a realistic long-term volatility with extremely large swings at large time scales. We also show that this rBergomi is not fast enough for calibration purposes, unlike the rough Heston which is highly tractable. Compared to standard stochastic volatility models, the rough Heston hence provides efficiently a more accurate fair value of long-term life insurance contracts embedding path-dependent options while being highly consistent with historical and risk-neutral data.

Keywords Rough volatility · Long-term volatility modeling · Equity-linked endowment valuation · SSVI parametrization · Long-term option pricing · Model calibration

✉ Jean-Loup Dupret
  jean-loup.dupret@uclouvain.be

Extended author information available on the last page of the article

1 Introduction

Standard stochastic volatility (SV) models such as the well-known Heston or Bates models have been introduced long ago to address the shortcomings of the celebrated model of Black & Scholes. However, such models are still limited and cannot reproduce some important empirical facts of the historical volatility and of the observed implied volatility surface.

In their seminal paper, Gatheral et al. [26] propose a model called *"Rough Fractional Stochastic Volatility"* (RFSV) where the log-volatility process is modeled in terms of a fractional Brownian motion. More precisely, a fractional Ornstein-Uhlenbeck process is used with $H < 1/2$, in contrast with the *"Fractional Stochastic Volatility"* model (FSV) previously introduced by Comte and Renault [15], where the Hurst index is assumed to satisfy $H > 1/2$. Gatheral et al. [26] find a highly consistent model with empirical estimates of the volatility time series. Moreover, the RFSV volatility process is stationary, which ensures reasonableness of the model in the long run. However, due to the need of Monte-Carlo simulations, this RFSV model does not provide rapidly option prices, nor an effective calibration procedure. More tractable pricing models such as the rBergomi from Bayer et al. [4] or the rough Heston from El Euch et al. [19] were then derived from the RFSV model to improve the efficiency of model calibration and option pricing. These two models appear to be extremely good at fitting the implied volatility surface while still reproducing the empirical properties of the historical volatility due to their rough sample paths. This paper shows how to expand these two rough-type models at larger time scales in order to price long-term life insurance contracts and explains why they provide a more accurate value of such contracts.

First, we will see that the stationary property of the volatility in the RFSV model will be lost when considering the rBergomi and rough Heston models. Despite this non-stationary property, we will manage to build for the rough Heston model a stable regime for the volatility in the long-run so as to price consistently long-term life insurance claims. On the contrary, for the rBergomi model, we will show that the generated volatility at large time scales will not be realistic and will tend to exhibit extremely large swings. Moreover, since these long-term properties of the rough Heston and rBergomi models depend heavily on the forward variance curve, we will show how to extrapolate the values of this curve beyond the observed maturities. In particular, we will derive a methodology based on a SSVI parametrization of the volatility surface which allows the forward variance curve to be consistent with the absence of static arbitrage and to be stable for large maturities. We will then verify practically these long-term properties by valuating an equity-linked endowment embedding a cliquet option (using four different models: Heston, Bates, rBergomi and rough Heston). This will allow to highlight the added-value of using rough-volatility models (and especially the rough Heston) for pricing such long-term life insurance contracts.

The main contribution of this paper is therefore to propose a calibration and a pricing methodology for long-term life insurance contracts using rough volatility

models. We also contribute with this work to highlight and study the divergent long-term properties between rough volatility models and standard SV models. This way, we will be able to explain why these rough volatility models provide a more consistent and accurate fair value of such long-term claims. We will indeed find a significantly different fair value of our equity-linked endowment with models incorporating rough volatility, especially at long time scales with the rough Heston model. In fact, we will see that this rough Heston model exhibits the best long-term properties while being highly tractable. This paper also aims to compare these models in terms of fit of the observed European option prices and implied volatility surface, which will confirm the high robustness of rough volatility models (and especially of the rough Heston model).

2 Life insurance contract

Our aim is thus to price the following equity-linked endowment using rough volatility models and compare them with standard SV models, such as the Heston and Bates models. We thus consider an insurance contract that provides a lump sum payment at maturity T in case of survival, or a payment at the time of death if it occurs before T. We first denote by τ_0 the random residual lifetime of the policyholder at time $t = 0$. We suppose an equity-linked case, where payment amounts depend on the market value of a reference fund $F(t)$ and where an amount $F(0)$ is invested in it at $t = 0$. We then introduce a yearly minimal guarantee κ_g for the policyholder and a maximal yearly return κ_m that this policyholder can earn on the fund. The survival benefit is then given by $F_T \, \mathbb{1}_{\tau_0 \geq T}$ and the death benefit by $F_{\tau_0} \, \mathbb{1}_{\tau_0 < T}$, where F_t is given by a series of guarantees (known as a cliquet option) for $t \in [0, T]$:

$$
\begin{aligned}
F_t = F_0 \prod_{u=1}^{\lfloor t \rfloor} \min & \left\{ e^{\kappa_m} \, ; \, \max \left\{ 1 + \pi \left(\frac{S_u}{S_{u-1}} - 1 \right) ; e^{\kappa_g} \right\} \right\} \\
& \times \min \left\{ e^{\kappa_m(t - \lfloor t \rfloor)} \, ; \, \max \left\{ 1 + \pi \left(\frac{S_t}{S_{\lfloor t \rfloor}} - 1 \right) ; e^{\kappa_g(t - \lfloor t \rfloor)} \right\} \right\}.
\end{aligned}
\tag{1}
$$

In the equation above, S_t is the price process of each fund unit defined on a filtration $(\mathcal{F}_t)_{t \geq 0}$. The cliquet above implicitly assumes yearly resettlements. Moreover, the rate π identifies the portion of yearly return recognized to the policyholder with $\pi \in (0, 1]$.

In this life insurance claim, we will model mortality using the following assumptions. We first introduce the non-homogeneous Poisson process $N_t := \mathbb{1}_{\tau_0 < t}$ defined on a filtration $(\mathcal{G}_t)_{t \geq 0}$, which is equal to zero as long as the individual is alive and jumps to one at death. We then assume independence between the mortality process N_t and the price process S_t. The intensity of N_t is given by the deterministic Makeham force of mortality $\mu_x(t) = c + ab^{x+t}$ for a policyholder aged x at time $t = 0$. Hence, her survival probability at time T, being alive at $t = 0$, is equal to

$$_T p_x = P(N_T = 0 \mid \mathcal{G}_0) = \exp\left(-\int_0^T \mu_x(u)\, du\right).$$

We now introduce the main characteristics of the RFSV model from Gatheral et al. [26] and then derive two tractable models from it, the rBergomi and the rough Heston models, that will help us to give a more consistent and accurate market value to this insurance contract.

3 Key features of the RFSV model

Gatheral et al. in [26] build the Rough Fractional Stochastic Volatility model (RFSV) with the following SDE under the real-world measure $\mathbb{P}$:

$$dS_t = \mu\, S_t\, dt + \sigma_t\, S_t\, dW_t, \tag{2}$$

$$d\log(\sigma_t) = \lambda(\theta - \log(\sigma_t))dt + \nu\, dB_t^H, \tag{3}$$

where μ is a drift term, W_t a standard Brownian motion and B_t^H is a fractional Brownian motion (fBm) with Hurst exponent H. W_t and B_t^H are in general correlated through the constant correlation ρ between W_t and the Brownian motion driving the Mandelbrot & Van Ness representation [32] of B_t^H. Recall that the sample paths of B_t^H are Hölder-continuous of order β for any $\beta < H$. Similarly, sample paths of B_t^H are almost surely nowhere Hölder-continuous of order β for any $\beta > H$. Therefore, the larger the Hurst exponent H, the smoother the sample paths and the lower the H, the rougher they are. More precisely, when $H < 1/2$, the sample paths of the fBm are called rough. Since $\log(\sigma_t)$ is driven in Eq. (3) by such fBm, the sample paths of $\log(\sigma_t)$ are also Hölder-continuous of order β for any $\beta < H$ and exhibit the same regularity behavior as B_t^H.

Given that Eq. (3) models the log-volatility as a fractional Ornstein-Uhlenbeck (fOU) process, we refer to Cheridito et al. [14] for the derivation of its stationary solution. One important property of the RFSV is that the volatility process σ_t itself generated by this model is again stationary, which ensures reasonableness of the model at large time scales when pricing long-term claims on the underlying. The cornerstone of [26] is to impose the Hurst exponent H of the fBm B_t^H to be in $\left(0, \frac{1}{2}\right)$ and a very long reversion time scale with $\lambda \ll 1/T$. Such conditions aim to generate rough sample paths and to introduce short-range dependence for the volatility process as explained by Gatheral et al. in [26]. Their findings are extremely consistent at any time scales with empirical statistical properties of the observed volatility time series as confirmed in Bennedsen et al. [7]. Firstly, Gatheral et al. show, for $\lambda \ll 1/T$ and $0 < H < 1$, that the log-volatility process $\log \sigma_t$ behaves locally as a fBm. Indeed, as $\lambda \to 0$, they prove that the log-volatility is close to the fBm B_t^H under the RFSV model (3). Therefore, this model approximately reproduces the well-known scaling property of the fBm (cfr Karatzas and Shreve [30]). This scaling property is clearly verified empirically for the discrete historical log-volatility process and

allows us to estimate the Hurst index H of the observed volatility process. Many studies (as in [7]) consistently find $H \approx 0.1$, which confirms the rough property of the historical volatility, *i. e.* a Hurst exponent $H < 1/2$. Secondly, neither the auto-covariance function $\text{cov}(\sigma_{t+\Delta}, \sigma_t)$ of the volatility process in the RFSV model nor the empirical counterpart of $\text{cov}(\sigma_{t+\Delta}, \sigma_t)$ decay as a power law (cfr *Figure 12* on *p. 941* in [26] with $\Delta > 0$). Therefore, these authors claim that historical volatility data are in accordance with the RFSV model, on the contrary to long memory models such as the FSV model of Comte and Renault [15].

Finally, the RFSV model is not only consistent with empirical statistical properties of the volatility time series but also with the observed implied volatility surface. Indeed, standard stochastic volatility models such as the Hull and White and Heston models do not provide a good fit of the volatility surface (especially for short expirations). Particularly, these models generate a term structure of at-the-money (ATM) volatility skew[1] under a risk-neutral measure $\mathbb{P}^*$ that does not match the observed one for small time to maturity $\tau = T - t$. Instead, empirical studies show that this observed term structure of ATM skew is well approximated by power-law functions of the form $\psi(\tau) \sim \tau^{H-1/2}$ with $0 < H < 1/2$, which can be generated by stochastic volatility models where the log-volatility is driven by fBm with values of the Hurst exponent in (0, 1/2). The explosion of the volatility skew as $\tau \to 0$ can therefore be modeled using fBm without introducing jumps in our model, as we will confirm in Sect. 5.

Although empirically and theoretically grounded, the RFSV does not allow to price rapidly option prices and therefore to calibrate effectively a pricing model. Indeed, we need Monte-Carlo simulations which are fairly slow, especially for calibration. Therefore, we now show how to adapt the RFSV to obtain more tractable models that can be used to price long-term claims on the underlying. We first analyze in more detail a simple case of the RFSV model when $\lambda = 0$, called the rBergomi model, built upon a forward variance curve. Secondly, we study an extension of the classical Heston model incorporating a rough fractional volatility process. This rough Heston model has the nice property of generating a realistic long-term behavior for the volatility process and of having a characteristic function of the log-stock price in quasi-closed form.

3.1 rBergomi model

First, let denote $v_u = \sigma_u^2$ the instantaneous variance at time u and the forward variance curve (also called variance swap curve) $\xi_t(u) = \mathbb{E}[v_u | \mathcal{F}_t]$, $u \geq t$. We can easily recover v_t from $\xi_t(u)$ as $v_t = \lim_{u \to t} \xi_t(u)$. Following Bergomi and Guyon [9], forward variance models are models that can be written as a function of this curve $\xi_t(u)$.

---

[1] Recall that the term structure of ATM volatility skew is defined by $\psi(\tau) := |\frac{\partial}{\partial k} \hat{\sigma}_t^{imp}(k, \tau)|_{k=0}$ where k is the log strike $k := \log S_t/K$ and where $\tau = T - t$.

From Bayer et al. [4], the rBergomi model is obtained from the RFSV model by setting $\lambda = 0$ in the log-volatility dynamic (3). Under this assumption and from the Mandelbrot & Van Ness representation [32] of the fBm, these authors show that the variance process v_u in the rBergomi model can be rewritten under the physical measure $\mathbb{P}$ as

$$v_u = \mathbb{E}^{\mathbb{P}}(v_u|\mathcal{F}_t) \exp\left(\eta\,\tilde{W}_t(u) - \frac{1}{2}\mathbb{E}^{\mathbb{P}}\left[|\eta\tilde{W}_t(u)|^2\right]\right) = \mathbb{E}^{\mathbb{P}}(v_u|\mathcal{F}_t)\,\mathcal{E}\big(\eta\tilde{W}_t(u)\big),$$

where $\tilde{W}_t(u) := \sqrt{2H}\int_t^u (u-s)^{H-1/2}\,d\hat{W}_s$ is a square-integrable continuous martingale with $\hat{W}_t$ a standard Brownian motion under $\mathbb{P}$. We also define the stochastic exponential $\mathcal{E} := \exp\left(\Phi - 1/2\,\mathbb{E}[|\Phi|^2]\right)$ with Φ a zero-mean Gaussian process. Finally, we define $\eta := 2\,v\,C_H/\sqrt{2H}$ where $C_H := \sqrt{\frac{2H\,\Gamma(3/2-H)}{\Gamma(H+1/2)\,\Gamma(2-2H)}}$.

Under an equivalent risk-neutral measure $\mathbb{P}^*$ (with a deterministic change of measure), the authors in [4] finally find for variance process in the rBergomi model

$$v_u = \mathbb{E}^{\mathbb{P}^*}[v_u|\mathcal{F}_t]\exp\left\{\eta\sqrt{2H}\int_t^u \frac{1}{(u-s)^{1/2-H}}dW_s^* - \frac{\eta^2}{2}(u-t)^{2H}\right\}, \qquad (4)$$

where W_t^* is a standard Brownian motion under $\mathbb{P}^*$ and where $\mathbb{E}^{\mathbb{P}^*}[v_u|\mathcal{F}_t]$ is the forward variance curve $\xi_t(u)$ observed on the market. In Eq. (4), it is important to note the presence at $t = 0$ of a Riemann-Liouville fBm $\int_0^u C_H\,(u-s)^{H-1/2}\,dW_s^*$ as defined in [13], with a Hurst index H that induces the rough behavior of the variance process v_u. In particular, its paths are $(H-\varepsilon)$-Hölder continuous, as classical fBm. Moreover, since $\mathbb{E}^{\mathbb{P}^*}[v_u|\mathcal{F}_t] \neq \mathbb{E}^{\mathbb{P}^*}[v_u|v_t]$, this model is non-Markovian. Nevertheless, given the state vector $\xi_t(u)$, which can in principle be computed from observed option prices (cfr section 4.3), the dynamics of the model are well-determined. Finally, the pricing model to be simulated under $\mathbb{P}^*$ is

$$\begin{aligned}
S_T &= S_0\,e^{rT}\,\mathcal{E}\left(\int_0^T \sqrt{v_u}\,dW_u^{*,S}\right), \\
v_t &= \xi_0(t)\,\mathcal{E}\big(\eta\,\tilde{W}_t^*\big) = \mathbb{E}^{\mathbb{P}^*}[v_t|\mathcal{F}_0]\,\mathcal{E}\big(\eta\,\tilde{W}_t^*\big),
\end{aligned} \qquad (5)$$

where $W_t^{*,S} = \rho\,W_t^* + \sqrt{1-\rho^2}\,W_t^{'*}$ and $W_t^{'*}$ a Brownian motion under $\mathbb{P}^*$, independent from W_t^*. We can hence model the leverage effect in the rBergomi model with $\rho < 0$. It is important to note that the assumption $\lambda = 0$ prevents us from having a stationary model for the volatility and the variance processes. Long-term behavior of the rBergomi model will be discussed more thoroughly in Sect. 3.3.

3.2 Rough Heston

A reminder of the standard Heston model is given in [24] for interested readers. Bergomi and Guyon in [9] show that this Heston model can be written in terms of the forward variance curve $\xi_t(u)$ (cfr Appendix) by

$$d\xi_t(u) = v e^{-\lambda(u-t)}\sqrt{v_t}\,d\hat{W}_t^*. \qquad (6)$$

Furthermore, from the classical Mandelbrot-van Ness [32] representation of the fBm, we clearly see that the kernel $(u - s)^{H-1/2}$ plays a central role in the rough dynamic of the fBm with $H < 1/2$. Indeed, as said above, one can show that the Riemann-Liouville fBm $\int_0^u C_H (u - s)^{H-1/2} d\hat{W}_s^*$ has Hölder regularity $H - \epsilon$ for any $\epsilon > 0$. Therefore, in order to allow for a rough behavior of the variance process in a Heston-type model, El Euch and Rosenbaum [21] naturally introduce the kernel $(u - s)^{H-1/2}$ in the risk-neutral stochastic differential equation of the Heston model with $C_H := 1/\Gamma(H + 1/2)$ as follows

$$v_u = v_t + \frac{\lambda}{\Gamma(H + 1/2)} \int_t^u \frac{\theta^t(s) - v_s}{(u - s)^{1/2-H}} \, ds + \frac{\nu}{\Gamma(H + 1/2)} \int_t^u \frac{\sqrt{v_s}}{(u - s)^{1/2-H}} \, d\hat{W}_s^*, \tag{7}$$

where $\theta^t(.)$ is assumed to be continuous, $\mathcal{F}_t$-measurable and represents a time-dependent mean reversion level. When $H = 1/2$, one can verify that we indeed recover the classical Heston model. It can also be shown that the trajectories of the volatility itself are almost surely Hölder-continuous of order $H - \epsilon$, for any $\epsilon > 0$.

Moreover, El Euch et al. show in [20] and [19] that $\lambda\theta^t(.)$ can be directly inferred from the forward variance curve observed at time t on the market $\xi_t(u)$. By doing so, they can rewrite the model (7) in the asymptotic setting $\lambda \to 0$ by

$$v_u = \xi_t(u) + \frac{1}{\Gamma(H + 1/2)} \int_t^u (u - s)^{H-1/2} \nu \sqrt{v_s} \, d\hat{W}_s^*. \tag{8}$$

Since the forward variance curve $\xi_0(u)$ at time $t = 0$ is observed (or at least can be retrieved) from the market, we only have three parameters left to estimate: H, ν and ρ. Reduction of parameters for the rough Heston is of utmost importance for improving the efficiency of the calibration methodology. Moreover, the fact that we consider $\lambda = 0$ implies that the average long-term behavior of the variance process in the rough Heston will be ruled by the forward variance curve $\xi_0(t)$ and not by the mean-reversion parameters λ and $\theta^0(\cdot)$ anymore (see Sect. 3.3 for more details). We also note that the limit $u \to t$ of the rough Heston makes no sense. This reflects the fact that this model (as the rBergomi) is not Markovian with respect to the current variance state v_t. However, it is directly visible from equation (8) that the rough Heston is Markovian in the forward variance curve $\xi_t(u)$. Finally, the rough Heston can also be expressed in the forward variance form as

$$d\xi_t(u) = \frac{\nu}{\Gamma(H + 1/2)}(u - t)^{H-1/2} \sqrt{v_t} \, d\hat{W}_t^*,$$

which is highly similar to (6), with the presence of a Riemann-Liouville kernel in addition.

Furthermore, from Gatheral and Keller-Ressel [27], we have that the Heston and rough Heston forward variance models are said to be affine. In both cases, they show that the characteristic function of the log-asset price $X_T = \log S_T$ at time t can be written as

$$\Phi_t(a, T) = \mathbb{E}\left[e^{iaX_T}|\mathcal{F}_t\right] = \exp\left(ia\big(X_t + r(T - t)\big) + \int_t^T \xi_t(s)\, g(T - s, a)\, ds\right),$$
(9)

where $g(\cdot, a) : \mathbb{R}_+ \to \mathbb{R}_-$ is the unique global continuous solution of a convolution Riccati equation (cfr [27]). In the classical Heston model, they find that

$$g(t, a) = \partial_t h(t, a) + \lambda\, h(t, a),$$

where $h(\cdot, a) : \mathbb{R}_+ \to \mathbb{R}_-$ is the unique C^1-function solving the Riccati ODE

$$\partial_t h(t, a) = -\frac{1}{2}a(a + i) - (\lambda - i\, a\, \rho\, v)h(t, a) + \frac{1}{2}v^2\, h(t, a)^2, \quad h(0, a) = 0. \quad (10)$$

In the rough Heston model with $\lambda = 0$, we have this time that $h(\cdot, a)$ is the unique continuous solution of the following fractional Riccati equation

$$g(t, a) = D^\alpha h(t, a) = -\frac{1}{2}a(a + i) + i\, a\, \rho\, v\, h(t, a) + \frac{1}{2}v^2\, h(t, a)^2, \quad I^{1-\alpha}h(0, a) = 0,$$
(11)

with D^α the Rieman-Liouville fractional derivative of order $\alpha = H + 1/2$ and $I^{1-\alpha}$ the Rieman-Liouville fractional integral of order $1 - \alpha$ (cfr [19]). This equation is exactly the same as in the classical Heston model (with zero-mean reversion) but with the time derivative replaced by a fractional derivative that makes the model rough.

We thus have a quasi-closed formula for the characteristic function in the rough Heston model since it is given by the simple expression (9). Contrary to the classical Heston case, the drawback is that there is no explicit solution to (11). However, this fractional Riccati equation can be solved numerically quasi instantaneously using the method described in Gatheral & Radoičić [28], built upon the combination of a short-time and an asymptotic expansion of the solution $h(t, a)$. As shown in [28], this method is particularly fast, simple and accurate to compute the approximate solution of the fractional Riccati equation (11). We refer to Section 5 of [28] for a more thorough discussion on the quality and convergence of their approximation for $h(a, t)$. Then, European option prices may be obtained efficiently from the characteristic function (9) using standard Fourier techniques such as the Carr-Madan formula [12]. Finally, this fractional Riccati ODE also allows to study portfolio insurance strategies, as developed in [18].

3.3 Long-term behavior of rBergomi and rough Heston models

The Riemann-Liouville fBm in Eq. (5) for the rBergomi and in Eq. (8) for the rough Heston is a non-stationary process with non-stationary increments (cfr [13]), which thus also makes the variance process of both models non-stationary. Hence, we need to verify whether the variance process exhibits a reasonable long-term behavior in the rBergomi and rough Heston models since we do not have this stationary property anymore as we have in the RFSV model with $\lambda \neq 0$ (which ensures reasonable and stable properties on the long-run for the RFSV variance process, cfr [26]). More

precisely, we have to make sure that this variance process (and particularly its two first conditional moments) do not explode for large maturities.

First, as shown in [16] and in [2], the Riemann-Liouville fBm can be represented as an infinite superposition of Ornstein-Uhlenbeck processes with different mean reversion speeds. Hence, even if $\lambda = 0$, authors in [1] show that there is an inherent mean reversion feature around the forward variance curve in rough volatility models coming from the Riemann-Liouville fBm. This mean-reversion property combined with an appropriate behavior of the long-end of the forward variance curve may thus allow for a sufficiently well behaved variance process at large maturity in rough volatility models, as we will see. For both the rough Heston and the rBergomi models, the fact that we consider $\lambda = 0$ implies that the average long-term behavior of the variance process will be ruled by the forward variance curve $\xi_0(t)$ and not anymore by the mean-reversion parameters λ and $\theta^t(\cdot)$ of Eq. (7) for the rough Heston, nor by the parameters λ and θ of Eq. (3) for the rBergomi. Indeed, this simply comes from the fact that the conditional mean of the variance process is now given by $\mathbb{E}^{\mathbb{P}^*}[v_u|\mathcal{F}_t] = \xi_t(u)$. Hence, we will discuss in Sect. 4.3 how to build such forward variance curves with non-exploding long-term behavior. However, long-term behavior of the variance process in both models is not solely driven by the form of this forward variance curve (since this curve only controls the average value of the variance process). The non-stationary Riemann-Liouville fBm has also a strong impact on the conditional variance of the variance process given by $\mathbb{V}_{\mathbb{P}^*}[v_u|\mathcal{F}_t]$, as explained in Appendix. Indeed, this quantity $\mathbb{V}_{\mathbb{P}^*}[v_u|\mathcal{F}_t]$ increases exponentially with u in the rBergomi model and hence tends to exhibit extreme values for large maturities (see Fig. 15). For the rough Heston model, the rate of increase of this quantity is much slower and hence, we do not observe this exponential growth of $\mathbb{V}_{\mathbb{P}^*}[v_u|\mathcal{F}_t]$ for the considered maturities, as again depicted on Fig. 15. The generated variance sample paths at large time scales are thus more reasonable and less volatile in the rough Heston while they exhibit extremely large swings for the rBergomi. This behavior will have an impact on the price of long-term life insurance claims as we will see in the last section of this paper.

4 Calibration

In this section, we will show how to build a consistent calibration methodology. We will then compare four models (Heston, Bates, rBergomi and rough Heston) in terms of fit of the observed European option prices and implied volatility surface for the CAC 40 index. We will mainly focus on the long-term behavior of such models and we will then use these calibrated models to price our equity-linked endowment embedding the cliquet option (1).

As in [26], we first provide a statistical estimation of the RFSV parameters based on historical data for the CAC 40 index from January 2004 to July 2020 (obtained from the Oxford-Man Institute). Using the scaling property of [26] to estimate the smoothness of the volatility process for the CAC 40, we find an estimated value $\hat{H} = 0.13$. The historical estimate of ν is also derived from this scaling property and is equal to $\hat{\nu} = 0.31$.

The aim of the calibration method is to find, for each model, the model parameters that match derivative model prices as best as possible with the observed market prices of vanilla derivatives in the market. It then boils down to an optimization problem where we have to find the minimum distance between model prices/model-based implied volatility and market prices/market implied volatility. In this paper, we choose to minimize the distance between model-based implied volatility $\widehat{\sigma}_j^{imp}$ and market implied volatility σ_j^{imp} since it leads to more stable results. Finally, we introduce the weighted Root Mean Square Error as the loss function, which is defined as

$$\text{RMSE} = \sqrt{\sum_{j=1}^{N} \frac{w_j}{N} \left(\sigma_j^{imp} - \widehat{\sigma}_j^{imp} \right)^2}, \qquad (12)$$

where $w_j = \frac{1}{\text{Ask}_j - \text{Bid}_j}$, *i. e.* the weight is the inverse of the bid-ask spread, expressed in terms of implied volatility. This way, we give more importance to observations with small bid-ask spread. Indeed, if an option is liquid, then its bid-ask spread is supposed to be small and its price/implied volatility is more accurate. Mathematically, it boils down to find the optimal set $\Theta^* \in \mathbb{R}^p$ of the p model parameters such that

$$\Theta^* = \arg\min_{\Theta} \mathcal{L}\big(\sigma^{imp}, \widehat{\sigma}^{imp}(\Theta) \big),$$

where $\mathcal{L}$ is the RMSE loss function. Finally, we highlight the fact that the results of the optimization methodology can be highly dependent on the initial parameters. Even for the Heston model, there is no consensus among researchers on whether the objective function for the calibration is convex or not, as explained in [17]. In any case, to overcome this problem of guessing the initial parameters, we use a global optimizer[2] combined with a local optimizer (the standard *nlminb* function in R). Indeed, global optimizers can find a solution on their own even without any initial guess while local optimizer need a suitable starting point. Therefore, we use the approach described in [35] which takes the final parameters provided by the global optimizer as initial values for the local optimization. This combination of global and local optimizers allows to refine the final parameters of the calibration and minimize the loss function, as explained and shown in [35]. However, even with this technique, we will see that the rBergomi model still appears to be highly unstable due to the need of Monte-Carlo simulations for this model.

4.1 Market data

We first choose as starting date $t = 0$, the 6th of July 2020. The maturity of vanilla options as well as the risk-free term structure will be defined with respect to this date.

---

[2] More precisely here, the Simulated Annealing (SA) algorithm of [37] with the package *GenSA* in R.

Firstly, the risk-free rates used for pricing purposes are derived from the observed swap term structure. The technique for constructing this swap term structure divides the curve into two term buckets. The short end of the swap term structure is built using interbank deposit rates. We will here consider EURIBOR rates from one day to 12 months. The long end of the risk-free interest rate curve (maturity above 1 year) will be based on the European swap term structure available from the EIOPA for the month of July[3]. Table 12 in Appendix provides a summary of the risk-free rates used between 0 and 20 years. The dividend yield is chosen to be 1% but this assumption does not have a significant impact on the results and conclusions of this paper.

Secondly, we have that the price S_0 at time 0 of the CAC40 index is equal to 5028.56 €. As mentioned above, we also need market prices of European options on the CAC40 in order to calibrate later our model since these are the most traded financial instrument in the equity world. Indeed, there are no liquid long-term products traded on the market on which we can calibrate our models for large maturities. The best we can hope so as to be the most-market consistent is therefore to reproduce as best as possible the observed implied volatility surface (and hence prices of European options) and then extrapolate the obtained trend for large maturities. In particular, we will see two methods below for obtaining the values of the forward variance curve beyond the available maturities. From Bloomberg, we thus gather a database that includes 366 European options with the option bid price and the option ask price for different strikes and maturities. The true market price is here considered as the mid value between the bid price and the ask price, which is a common assumption. Using the one-to-one relationship between market prices and implied volatility from the Black and Scholes formula, we can build a database with the bid, ask and mid implied volatility for each strike and maturity. We then apply the following common filters as in Moyaert and Petitjean [34] and select the following options:

– **Out-of-the-money options**: Since out-of-the-money options are more actively traded than in-the-money options (as a protection), the quotes on out-of-the-money options are usually more reliable.
– **The bid-ask spread** (on the option prices) is less than 5%. Otherwise, we consider that there is no sufficient liquidity to take the option into account.
– **Maturity:** We reject options with maturity equal to 0.9 year due to data quality issue for this particular maturity.

We have a final database of 145 OTM options for which we can observe the strike, the maturity, the bid, ask and mid implied volatility. We now turn to the specific calibration method for each model. Indeed, even if the general methodology is the same, the way we price our European options will vary depending on the model.

---

[3] Further information on risk-free rates computation can be found at: https://www.eiopa.europa.eu/tools-and-data/risk-free-interest-rate-term-structures_en.
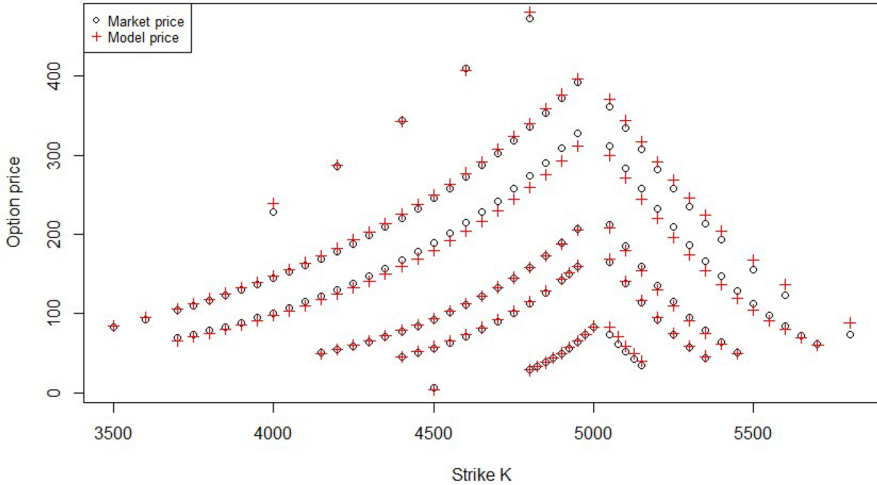
Fig. 1 Comparison of Heston option prices in red crosses vs. market option prices in black dots (CAC 40)

4.2 Heston and Bates models

We have at disposal for these two models a closed-form expression for their characteristic function, as reviewed in [24]. Then, for a given maturity, the Carr-Madan formula [12] generates prices of European options for a whole range of strikes in one run very fast using Fourier inversion. By calling many times this pricing algorithm on the available maturities in the data, we can thus find the optimal parameters of each model.

- **Heston**

A reminder of the standard Heston model is given in [24]. The set of initial parameters obtained from the Simulated Annealing algorithm is given by (0.2898, 2.9176, 0.0966, 1.4703, −0.7010). Using the local optimizer *nlminb* in R, we then find a minimal RMSE of 0.11694 with the following final parameter values Θ^*:

σ_0^*	λ^*	θ^*	v^*	ρ^*
0.28992	2.91760	0.09664	1.47027	-0.7010

We see that we have a high speed of mean reversion λ^* and a high level of the vol-of-var parameter v^* which implies large swings in the variance process. We also obtain a large negative correlation between the stock process and the variance process, which is consistent with the leverage effect. Finally, the mean reversion level θ^* towards which the variance will converge is 9.66% (which represents a volatility of 31,09%). It is no wonder to obtain this high level of volatility as well as vol-of-var
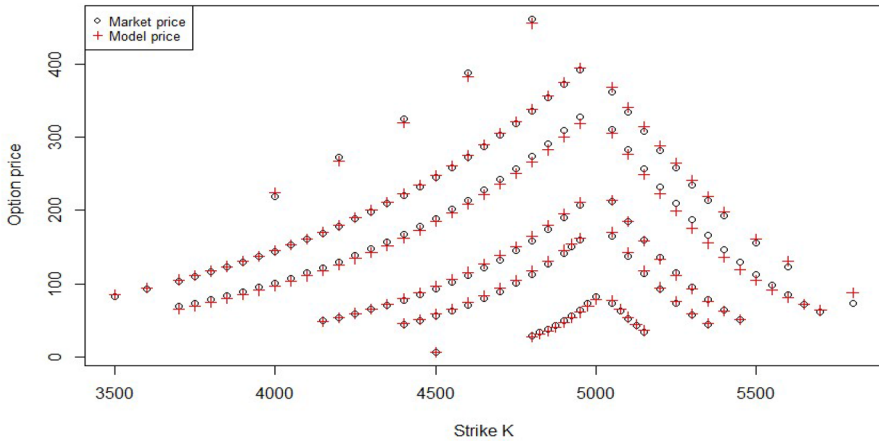
Fig. 2 Comparison of Bates option prices in red crosses vs. market option prices in black dots (CAC 40)

parameter given the state of the economy due to the COVID-19 outbreak in July 2020. Finally, the Heston model with the parameters obtained above leads to Fig. 1 when compared to market prices of European options on the CAC 40 index.

The calibration of the forward-variance specification of the Heston model, as described in [9] and [10], is provided in Appendix. This appendix will allow to compare more thoroughly the Heston model with rough volatility models which are also based on this forward variance curve.

- **Bates**

For a reminder of the Bates (or SVJ) model, we refer to [24]. The set of initial parameters obtained from the SA global optimizer is given by (0.27, 0.62, 0.12, 1.24, −0.66, −0.10, 0.11, 0.82). Using our local optimizer, we then find a minimal RMSE of 0.08465 with the following final parameter values Θ^*:

σ_0^*	λ^*	θ^*	ν^*	ρ^*	μ_j^*	σ_j^*	λ_j^*
0.2589	0.1555	0.2709	1.1593	-0.6640	-0.1004	0.1072	0.9080

Firstly, the RMSE is substantially lower than the one obtained with the Heston model, which means that the Bates model provides a better fit of the observed European option prices. The mean-reversion speed λ^* and the volatility of variance parameters ν^* are also lower, which implies that the swings in the variance process are less pronounced than in the Heston model. Moreover, we now observe jumps in the price process that are on average negative since $e^{\mu_j + \sigma_j^2/2} - 1 < 0$. The annual frequency of these jumps is equal to 90.8%. Finally, we observe that the long-run variance θ^* is higher than in the Heston model. This Bates models leads to Fig. 2 when compared to the observed market prices. The fit is clearly better than in the Heston model as said above. More precisely, we see that this improvement comes from the
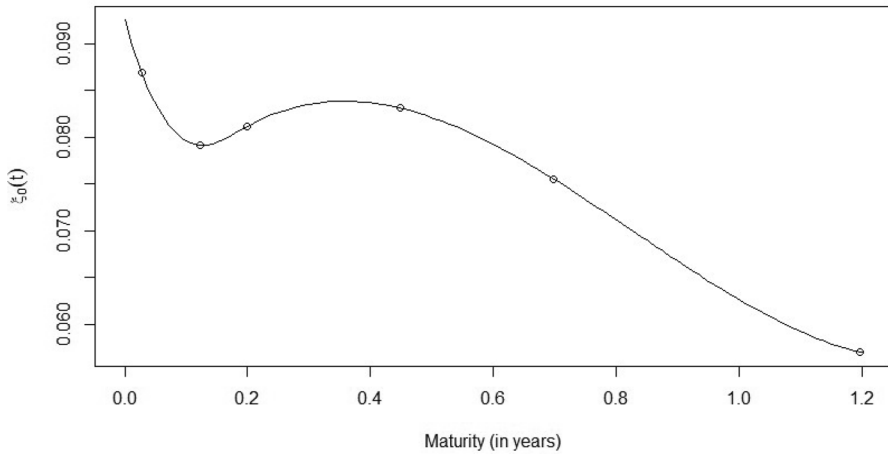
Fig. 3 Initial market forward variance curve $\xi_0^{mkt}(t)$ between 0 and 1.2 years

better fit of OTM call options with large maturities when using the Bates model. However, we also observe on Fig. 2 that option prices with the third largest maturity ($T = 0.45$) are still significantly out-of-market.

Note that the presence of jumps makes the calibration of the forward-variance specification of the Bates model really difficult and time-consuming. Indeed, the characteristic function of the Bates model cannot be written as an integral of the forward variance curve as in the Heston and rough Heston case with equation (9) since the Bates model is not an affine forward variance model due to its jump term (cfr [27]). We will therefore not consider this specification in this paper.

4.3 Rough Heston calibration

As explained above, we have a quasi-closed form for the characteristic function of the log-price X_t under the rough Heston model (8). We can then apply exactly the same calibration technique as for the Heston and Bates models described in the previous section. However, recall that the rough Heston is not Markovian in the current variance state v_t but Markovian in the (forward) variance swap curve $\xi_t(u)$. Hence, the rough Heston's characteristic function depends on this variance swap curve. In practice however, the variance swap curve $\xi_0(u)$ at time $t = 0$ is not obtained directly from the financial markets. Indeed, it is hard to obtain high-quality variance swap data since variance swaps are OTC contracts as explained in [4]. We thus choose to proxy the value of a variance swap of maturity T by the value of a log-contract (also of maturity T), as described for example in Chapter 11 of Gatheral [24]. Therefore, even if variance swaps are OTC contracts, we can obtain variance swap prices directly from the observed European options which are heavily traded on the market. This way, we can consider in this context that variance swap quotes derived from our European options are also reliable. The first method to obtain the initial variance swap curve is therefore to calibrate it based on our dataset of observed option

prices for the CAC 40. We hence obtain in Fig. 3 the following market variance swap curve, denoted $\xi_0^{mkt}(t)$, between 0 and 1.2 years when interpolated between observed maturities.

However, we only have European options with observed maturities until 1.2 years. In order to price long-term claims on the underlying, we need to extrapolate the values of $\xi_0^{mkt}(t)$ beyond 1.2 years and hence, we need to consider a term-structure parametrization of $\xi_0^{mkt}(t)$. Since the forward variance curve is estimated from the data and is not an output of the model, the average long-time behavior of the variance process is embedded in this forward variance curve parametrization (cfr Sect. 3.3). Indeed, recall that the forward variance curve controls the average value of the variance process v_t since $\xi_0(t) := \mathbb{E}^{\mathbb{P}^*}[v_t|\mathcal{F}_0]$. The long-end of this curve will thus have a strong impact on the behavior of the model for large maturities and we hence need to avoid parametrizations generating explosive or unrealistic forward variance curves. Otherwise, the variance process (and hence also the price process) will tend to explode when the maturity increases. The easiest way to achieve this is to impose a constant long-term value for the initial forward variance curve $\xi_0^{mkt}(t)$. Therefore, it is reasonable to choose a parametrization with asymptotic line such that

$$\lim_{t \to \infty} \xi_0^{mkt}(t) = cst \, .$$

This assumption allows the variance process of the rough Heston to be in a stable regime for large maturities. A classical choice for such parametrization is the Gompertz function

$$\xi_0^{mkt}(t) = z_1 e^{-z_2 \, e^{-z_3 \, t}} \, , \tag{13}$$

where z_1 is the asymptote, z_2 sets the displacement along the x-axis (here, the time to maturity) and z_3 sets the growth rate. Fitting the Gompertz function to the observed forward variance curve, we find:

$$z_1 = 0.03954 \qquad z_2 = -0.7992 \qquad z_3 = 0.5672$$

Therefore, the asymptotic level of the volatility is given by $\sqrt{0.03954} = 19.88\%$. Finally, combining the curve obtained in Fig. 3 with the Gompertz fit for $\tau > 1.2$, we obtain the initial market forward variance curve $\xi_0^{mkt}(t)$ in Fig. 4. We can observe that we enter a stable regime as of the 6th year.

Yet, we are aware that calibrating such Gompertz function based on only 6 different maturity points can seem dubious. Indeed, estimating an asymptotic value for the forward variance from the information carried out by short-maturity option data does not provide a lot of confidence in our results. Moreover, this way of building and extrapolating the forward variance curve does not ensure to avoid static arbitrage. Therefore, we now show how to tackle both of these issues. A better alternative to estimate the forward variance curve is to fit the SSVI parametrization [25] of the observed implied volatility surface and compute the forward variance curve associated with this parametrization. A brief reminder of such arbitrage-free SSVI parametrization is given in Appendix. The advantage
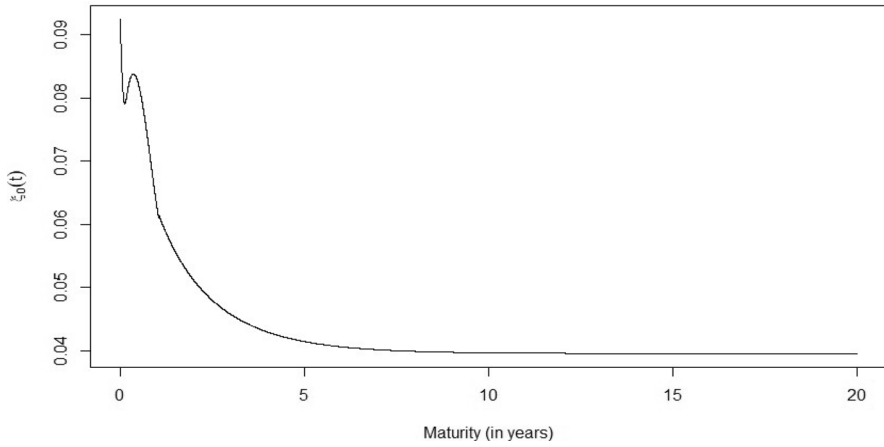
Fig. 4 Initial market forward variance curve $\xi_0^{mkt}(t)$ until $t = 20$ years
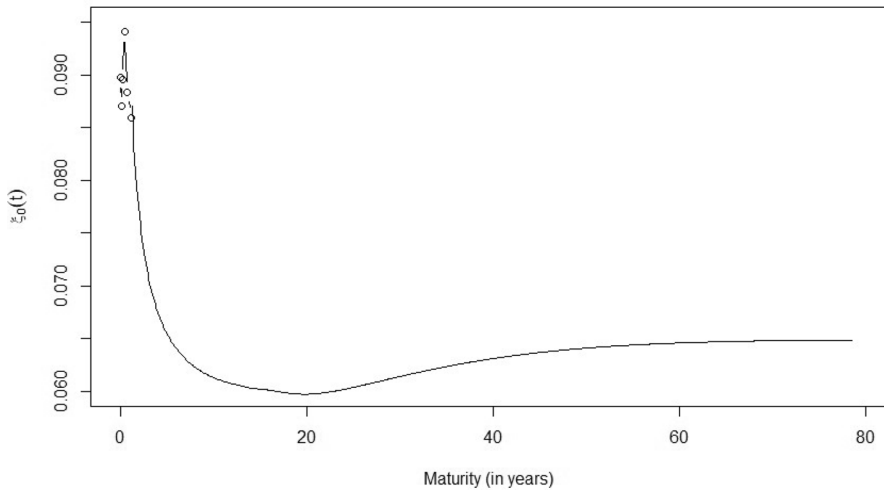

Fig. 5 Initial SSVI forward variance curve $\xi_0^{SSVI}(t)$ until $t = 80$ years. Black circles are the variance swap values for the available maturities

of this procedure is to ensure that the estimated forward variance curve is consistent with the absence of calendar spread and butterfly arbitrages. Furthermore, the extrapolation of the forward variance curve does not require to specify a particular function for this curve anymore since its extrapolation beyond 1.2 years in the SSVI parametrization only relies on an arbitrage-free argument, as explained in Appendix. We therefore do not need anymore to determine a long-term value of $\xi_0(t)$ based solely on short-term maturity data. We obtain this way the following SSVI forward variance curve $\xi_0^{SSVI}(t)$ depicted on Fig. 5.

We see that this forward variance curve $\xi_0^{SSVI}(t)$ tends to approximately exhibit the same shape as the market forward variance curve between 0 and 80 years. Moreover, the SSVI forward variance curve appears to be stable and does not explode for large maturities, which also ensures a stable regime and a reasonable average behavior of the rough Heston model on the long-term.

The last alternative we will consider is to use a constant forward variance curve denoted $\xi_0^{cst}(t)$. We decide arbitrarily to fix $\xi_0^{cst}(t) = \xi_0^{mkt}(0) = 0.0925$, $\forall t$. Note that this constant level is very close to the long-term mean θ^* obtained in the Heston calibration ($= 0.0966$). This parametrization for the forward variance curve will hence allow to compare more thoroughly rough volatility models with the latter. Results for calibration and pricing with $\xi_0^{cst}(t)$ are given in Appendix.

The SSVI forward variance curve being arbitrage-free, more reliable and more consistent, we now perform the calibration of the rough Heston model based on $\xi_0^{SSVI}(t)$. Results for the market and the constant forward variance curves are given in Appendix. Using the Carr-Madan formula [12] and the numerical approximation of Gatheral & Radoičić [28] for the fractional Riccati equation (11), we obtain in a first step the following set of initial parameters from the SA global optimizer: (0.1702, 0.6241, −0.6724). Using our local optimizer, we then find a minimal RMSE of 0.08457 with the following (same) final parameter values Θ^*:

H^*	ν^*	ρ^*
0.1703	0.6241	-0.6725

Based on the RMSE, we then have a slightly better fit than with the Bates model. It is impressive knowing that the rough Heston model in the asymptotic setting $\lambda \to 0$ has only 3 effective parameters to estimate while the Bates model has 8 parameters ! We will also analyze in the next section which of the models best fits the behavior of the implied volatility surface (and particularly the term structure of ATM skews). Moreover, it is important to note that the Hurst index H^* obtained via the risk-neutral calibration method is consistent with the Hurst index obtained via statistical estimation (under the real-world measure) equal to 0.13. Yet, we have a higher ν^* than the one estimated based on the historical time series ($= 0.31$) due to the market price of risk included in the risk-neutral valuation. Finally, we obtain a leverage effect of the same order as in the Heston and Bates models. Figure 6 depicts the fit of the rough Heston options prices compared with the observed market prices of European options.

4.4 rBergomi Calibration

The calibration of this model departs significantly from the three models described above. Indeed, no characteristic function is available in (quasi-)closed form. We then rely on Monte-Carlo simulations with the Hybrid scheme of [8], as applied in [33], to calibrate the parameters ρ, η and H of the rBergomi model under $\mathbb{P}^*$. More precisely, since the Riemann-Liouville fBm is a special case of Brownian Semistationary (BSS) processes, we follow the papers of Bennedsen et al. [8] and of McCrickerd
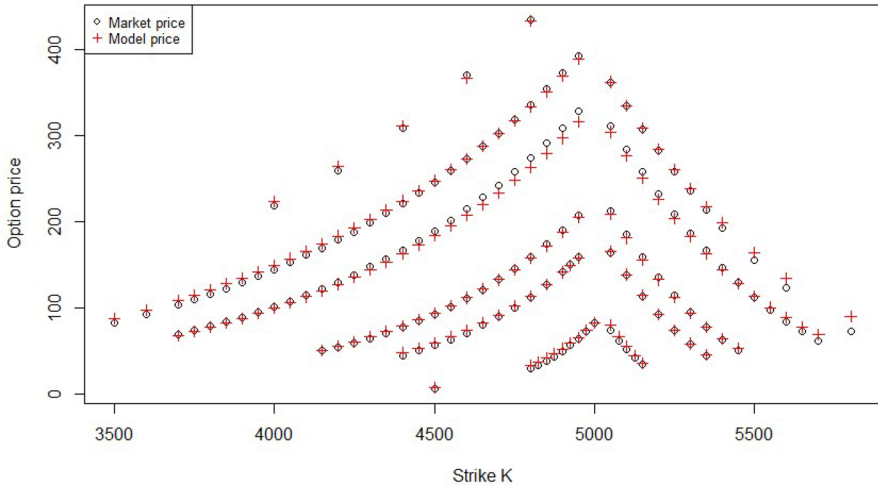
Fig. 6 Comparison of rough Heston option prices vs. market option prices (CAC 40)

et al. [33] in order to improve the efficiency of simulations in the rBergomi model. Note that the initial forward variance curve is exactly the same as the one derived in the calibration of the rough Heston model. Hence, we will again use $\xi_0^{SSSI}(t)$ in this section.

We find a RMSE of 0.08631 with the initial set of parameters equal to (0.15, 1.67, −0.92). This leads to the following final values Θ^*:

H^*	η^*	ρ^*
0.1515	1.6803	-0.9275

First, the RMSE is slightly higher compared with the rough Heston and Bates models but lower than the Heston model. We see that the calibrated Hurst exponent H^* is lower than the one found in the rough Heston model and closer to the historical estimate (= 0.13). Based on a $\eta^* = 1.6803$, we find the corresponding v^* equal to $\eta^* \sqrt{2H^*}/(2C_H) = 0.9969$. Therefore, the volatility of variance parameter v^* clearly needs to be much higher than the historical $\hat{v}$ to better fit the European option data (again due to the volatility of variance risk premium). The anti-correlation between the stock process and the variance process is stronger than the ρ^* derived from the rough Heston. Moreover, it is important to add that these results are quite unstable from simulation to simulation. The hybrid scheme is indeed not yet fast enough to provide a reliable calibration method, at least in our implementation. We used $m = 1,000,000$ and $\Delta t = t_k - t_{k-1} = T/n$ with $n = 400$ and the optimization was done in more than 5 h with these parameters. We need to increase m and decrease Δt to obtain more precise and stable results but it then requires far more computing time and memory, which is not suitable and tractable in practice. We then obtain Fig. 7 where we can see that the OTM puts are substantially off-market with this model.
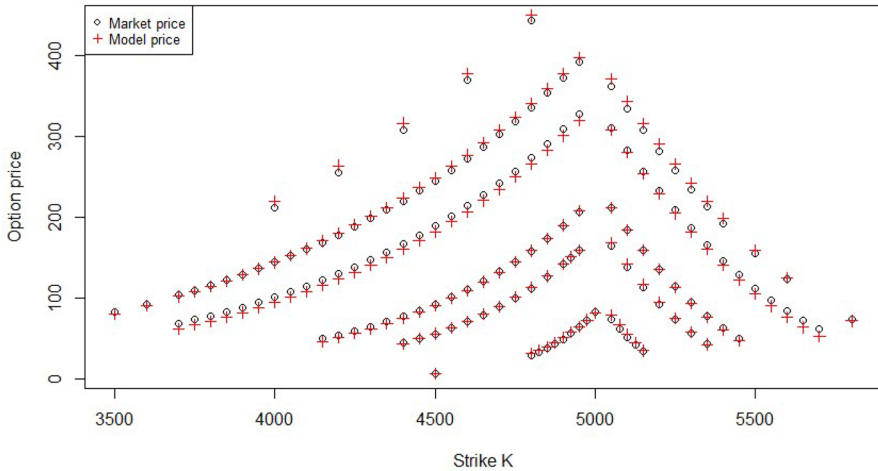
Fig. 7 Comparison of rBergomi option prices vs. market option prices (CAC 40)

Finally, recall that the SSVI parametrization of the forward variance curve ensures that in the long term we have on average a stable and non-exploding variance process in the rBergomi and rough Heston models (cfr Fig. 5). Nevertheless, we said that the presence of the non-stationary Riemann-Liouville fBm in both models also impacts the long-term behavior of the variance process. More precisely, if we now compare the conditional variance of the variance process $\mathbb{V}_{\mathbb{P}*}[v_u|\mathcal{F}_t]$, we obtain an increasing quantity in u with divergent properties between the two models as shown and explained with Fig. 15 in Appendix and with the corresponding equations 17 and 18. Clearly, the exponential growth of $\mathbb{V}_{\mathbb{P}*}[v_u|\mathcal{F}_t]$ in the rBergomi model does not allow for a reasonable behavior of the variance process in the long term with the calibrated parameters above. The same extreme behavior is obtained using the parameters of the rBergomi model found in the initial paper [4] and in [6]. On the contrary, the conditional variance $\mathbb{V}_{\mathbb{P}*}[v_u|\mathcal{F}_t]$ in the rough Heston exhibits an almost constant behavior for large times to maturity and is hence more appropriate for long-term pricing. This stable regime of the rough Heston model is also obtained using standard parameters such as in [19]. The impact of the quantity $\mathbb{V}_{\mathbb{P}*}[v_u|\mathcal{F}_t]$ on the price of life insurance claims for large maturities u will be analyzed more thoroughly in the last section.

5 Volatility surface fit

We now compare the Heston, Bates, rough Heston and rBergomi models in terms of implied volatility surface fit. More precisely, we will look at the fit of the term structure of ATM volatility skew $\psi(\tau)$ and confirm that rough volatility models provide a better fit.
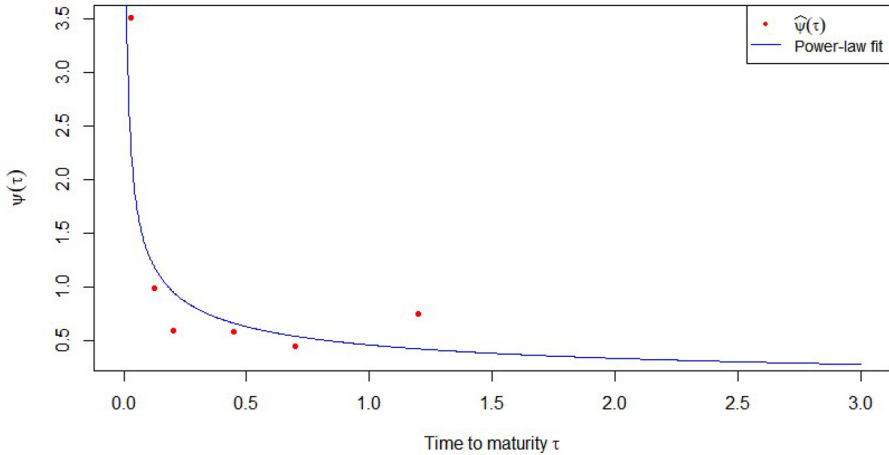
Fig. 8 Red dots are the ATM volatility skews $\widehat{\psi}(\tau)$ estimated for the available maturities. The power-law fit is superimposed in blue

From our market option prices database, we can build the term structure of ATM volatility skew $\psi(\tau)$. First, recall that $\psi(\tau) := \left| \frac{\partial}{\partial k} \hat{\sigma}_t^{imp}(\tau, k) \right|_{k=0}$ with k being the log-strike and $\tau = T - t$ the time to maturity. We can approximate it by

$$\widehat{\psi}(\tau) = \left| \frac{\hat{\sigma}_0^{imp}(\tau, k + \delta) - \hat{\sigma}_0^{imp}(\tau, k - \delta)}{2\delta} \right|_{k=0},$$

for small enough δ and for each available time to maturity τ. We then obtain in Fig. 8 the term structure of ATM volatility skew for our data at time $t = 0$.

The red dots are the estimated ATM skews for each of the available maturities. We clearly see that we obtain a term structure of ATM volatility skew which is consistent with the power-law function. Indeed, the blue line is the power-law fit to the data, obtained by the following linear regression:

$$\log \psi(\tau) = -\alpha \log \tau.$$

We find $\hat{\alpha} = 0.4546$. From Sect. 3, we know that $\psi(\tau) \sim \tau^{H-1/2}$ holds for the RFSV model. Hence, we have that $\hat{H}_{ATM} = 1/2 - \hat{\alpha} = 0.0452$, which is lower than the Hurst exponent estimated with historical data (but again rough !). However, we do not have a lot of different maturities in our option data set, which prevents us from having a consistent estimator $\hat{H}_{ATM}$ using this power-law fit. Therefore, we will mainly focus our analysis on the shape of the ATM skew term structure and on whether our different models are able to approximate this blue line rather than on the exact fit.

5.1 Comparison of the fit

We now compare the empirical term structure of ATM volatility skew with the term structures derived from each model. We first analyze the fit of the standard Heston and Bates model thanks to Fig. 16 in Appendix. The blue line is again the power-law fit of the observed ATM skews (with $\hat{\alpha} = 0.4546$). The green dots are the ATM skews $\hat{\psi}(\tau)$ derived from the different models for the available maturities. For the Heston model, we clearly observe that it does not allow to capture the high values of ATM skews for short maturities and hence, it cannot reproduce the power-law shape of $\hat{\psi}(\tau)$. This was indeed one of the issues of this model that we rose in Sect. 3. For $T > 0.20$, we can however note that the Heston fit approximates quite well the empirical blue line. Concerning the Bates model, the presence of jumps only provides a slightly better fit of the ATM skews $\hat{\psi}(\tau)$ compared with the Heston model. Indeed, the Bates model is still not able to capture the explosion of the ATM skews for very short time to maturity. This is due to the fact that the parameter λ_j controlling the frequency of jumps is only of 0.91 and that the average size of the jumps is also rather low. A higher value of λ_j or of $|\mu_j|$ would allow to better capture this explosion phenomenon for $\tau \to 0$.

We now analyze the fit of the rough Heston and the rBergomi models since we said that rough volatility models should be able to better capture the high curvature of $\hat{\psi}(\tau)$ for small time to maturity thanks to the rough behavior of their volatility process. We obtain Fig. 17 in Appendix. We clearly see that the green dots of both figures (*i. e.* the rough Heston and rBergomi fit for available maturities) exhibit the same shape as the blue line and can therefore be fitted by a power-law function of the form $\tau^{H-1/2}$. If we had at disposal even shorter maturities, the rough Heston and rBergomi models would likely better capture the explosion of $\hat{\psi}(\tau)$ for $\tau \to 0$. We can finally conclude that rough volatility models are more consistent with the observed term structure of ATM volatility skew than standard SV models.

6 Simulation and discretization methodology

In order to price the above equity-linked life insurance contract, we first need to explain how we can discretize and simulate sample paths of the price process and the variance process under our different models.

- Heston

Once the Heston model has been calibrated and the optimal parameters $\sigma_0, \lambda, \theta, \nu$ and ρ have been found, we can use a Monte Carlo approach to simulate the sample paths of the Heston model. We first simulate the stock price process and the variance process by generating correlated $N(0, 1)$ random numbers ε_S and ε_v (with correlation ρ). The relationship between ε_S and ε_v can be written as

$$\varepsilon_{v,t_i} = \rho \, \varepsilon_{S,t_i} + \sqrt{1 - \rho^2} \, \varepsilon'_{t_i},$$
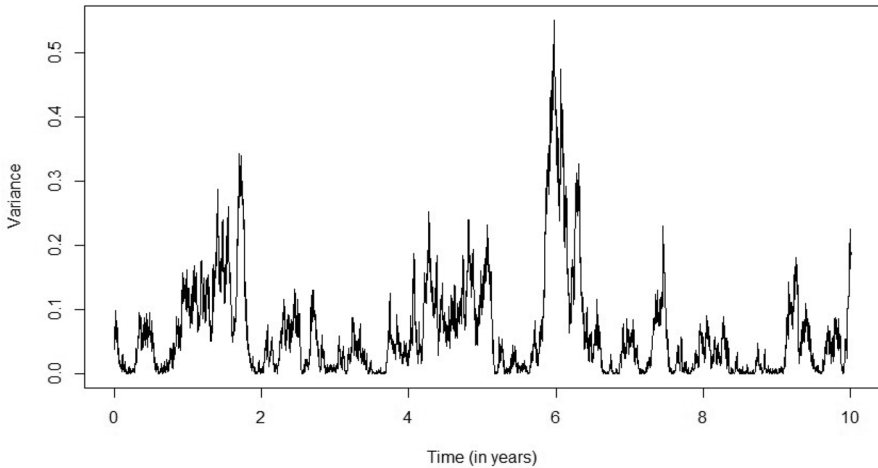
Fig. 9 One sample path of the variance process under the standard Heston model

where ε_{S,t_i} and ε'_{t_i} are independent $N(0, 1)$ random variables. Using an Euler discretization scheme for the price process and the variance process, we have

$$S_{t_{i+1}} = S_{t_i}\left(1 + r\Delta t + \sqrt{v_{t_i}}\sqrt{\Delta t}\,\varepsilon_{S,t_i}\right), \qquad (14)$$

$$v_{t_{i+1}} = v_{t_i} + \lambda(\eta - v_{t_i})\Delta t + v\sqrt{v_{t_i}}\sqrt{\Delta t}\,\varepsilon_{v,t_i}, \qquad (15)$$

for $i = 0, ..., n - 1$, with $t_0 = 0$ and $t_n = T$, where n is the number of time steps and $\Delta t = T/n$, for a given maturity T. We then simulate m sample paths of this stock price process and of this variance process. Now that we have the full path of $(S_{t_i})_{i=0,...,n}$ for each m, we can price path-dependent options, such as the cliquet option (1). In practice, the variance can become negative under a simulation because of the discretization. We then use the full truncation scheme of Lord et. al [31] to tackle this problem since it overcomes other Euler fixes (absorption, relfection, etc.) and quasi-second order schemes (Milstein scheme, Ninomiya and Victoir scheme [36], etc.) in terms of positive bias. The full truncation scheme therefore better reproduces the true properties of the CIR process. This simulation methodology gives us the following Fig. 9, depicting one sample path of the variance process under the standard Heston model over 10 years. We can clearly see the effect of the high volatility of variance (vol-of-var) parameter v with large swings in the variance process.

- Bates

We again use the Euler scheme with a full truncation fix for the variance process as in the Heston model. However, the discretization scheme of the price process is replaced by
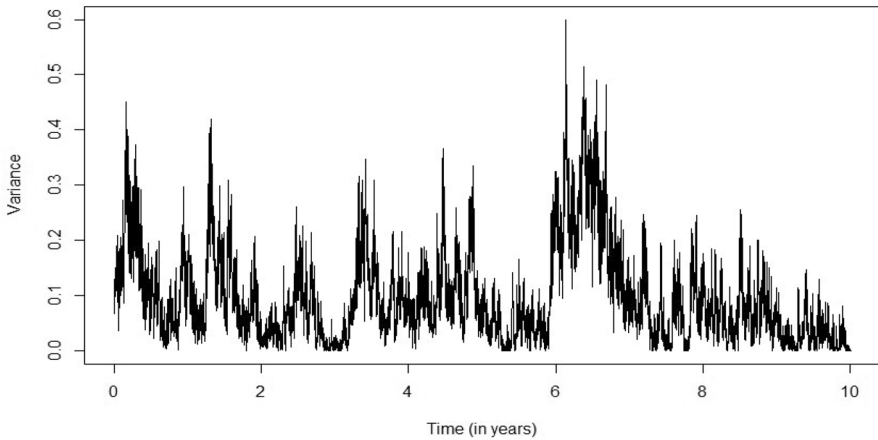
Fig. 10 One sample path of the variance process under the rough Heston model

$$S_{t_{i+1}} = S_{t_i}\left(1 + r\Delta t + \sqrt{v_{t_i}}\sqrt{\Delta t}\,\varepsilon_{S,t_i} + (Y_i - 1)\,\Delta N_{t_i}\right), \tag{16}$$

where $Y_i \sim LogN(\mu_j, \sigma_j^2)$ and $\Delta N_{t_i} \sim Poi(\lambda\Delta t)$.

Rough Heston

The discretized price process is exactly the same as in the Heston model with (14). However, due to the non-Markovian nature of the variance process under the rough Heston, an Euler discretization scheme for simulating v_t is very slow and does not allow to use the full truncation fix in order to deal with negative variance. A more time-efficient simulation scheme for the rough Heston can be found instead in [1] with a lifted version of the Heston model. This lifted Heston model appears to be a multi-factor approximation of the rough Heston model built as an infinite superposition of square-root (CIR) processes with the same dynamic but mean reverting at different speeds (cfr Sect. 3.3). Such infinite-dimensional Markovian representation of the limiting rough variance process is an appealing trade-off between flexibility and tractability, as explained in [1]. In practice, only few factors are sufficient which drastically speeds up the simulation procedure compared to an Euler discretization scheme. Moreover, this representation in terms of square-root processes allows to use the full truncation fix of [31] described above in order to avoid negative variance and to better reproduce the true properties of the variance process. For simulating our rough Heston model, we take the suggested values of the lifted Heston model defined in [1]: $\tilde{n} = 20$ factors and $r_{20} = 2.5$. The function $g_0^{\tilde{n}}(t)$ of this lifted Heston model is chosen so as to match the forward variance curve $\xi_0(t)$ and the speed of mean-reversion λ is again set to 0 since mean reversions at different speeds are inherent in the lifted Heston model. This parametrization allows to recover the rough Heston model (8) with its 3 effective parameters.
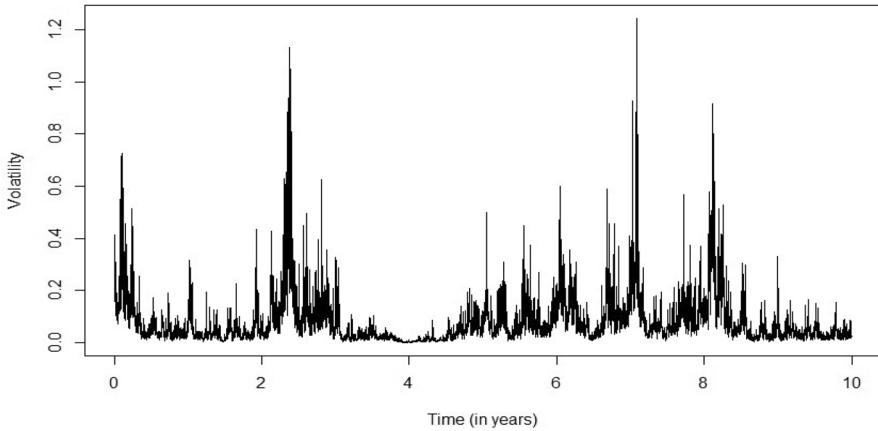
Fig. 11 One sample path of the variance process under the rBergomi model

One sample path of the variance process over 10 years under our calibrated rough Heston model with SSVI forward variance curve is plotted in Fig. 10. We clearly see the rough behavior of the variance process compared to the sample paths of the Bates and Heston models. We also have that the vol-of-var parameter ν is quite high, leading to large movements in the variance process.

rBergomi

The price process is again given by (14). However, the variance process is now simply given by

$$v_{t_i} = \xi_0(t_i)\,\mathcal{E}\Big(\eta\,\tilde{W}^*_{t_i}\Big),$$

where we use the SSVI forward variance curve for $\xi_0(t_i)\,(=\mathbb{E}^{\mathbb{P}^*}[v_{t_i}])$ and the hybrid scheme of [33] and [8] for the simulation of $\tilde{W}^*_{t_i}$, with $i = 0, ..., n$. The way the variance process is defined in (5) under the rBergomi model prevents us by definition from having negative variance. You can also find in Fig. 11, one simulated sample path of the rBergomi variance process using this Hybrid scheme. Due to the huge vol-of-var parameter η, the variance paths tend to explode and exceed 100%. Generated sample paths with the rBergomi are therefore not realistic. Furthermore, if we compute the sample variance $\mathbb{V}_{\mathbb{P}^*}[v_t]$, we would obtain the exact same shape as in Fig. 15, which confirms the extreme variability of the rBergomi variance process for large maturities. The roughness of the variance process is again clearly visible in Fig. 11.

7 Conclusion of the fit

From the analyses of the implied volatility surface, we can conclude that rough volatility models with the rough Heston and the rBergomi clearly outperform standard SV models in terms of goodness of fit of the observed term structure of ATM

volatility skew. Therefore, with the lowest RMSE (0.0846) and a good fit of the implied volatility surface, we conclude that the rough Heston model is the best of the considered models at reproducing the observed risk-neutral data. Secondly, since the rough Heston exhibits a rough variance process (with a H close to the historical estimate), this model can also better reproduce at any time scales numerous statistical properties of the historical volatility process. Therefore, the fact that this model exhibits rough volatility and hence better reproduces the empirical properties of the historical volatility will lead to a better price of insurance contracts at large time scales. More precisely, the parameter H controlling the roughness/memory of the variance process has a direct impact on long-term life insurance contracts since the generated sample paths of the fund's underlying price process S_t will strongly vary in function of this index H (as shown below in Sect. 8 and Appendix). In fact, the larger the maturity, the more important will be the effect of the roughness of the variance process on the fair value of such contracts. Moreover, as shown in Sect. 4.3, we can build at large time scales a stable regime for the variance process in the rough Heston, which ensures a reasonable long-term behavior of the model. Combined with the fact that the SSVI forward variance curve $\xi_0^{SSVI}(t)$ is consistent with the absence of arbitrage at any time scales, we will obtain in the next section a very reliable and consistent fair value of long-term life insurance contracts. Finally, the rough Heston is also particularly tractable (only three parameters to calibrate and a characteristic function available in quasi-closed form) which is very important in practice for time-efficient calibration and option pricing.

Concerning the rBergomi model, even with calibrated parameters, it provides a slightly higher RMSE than the rough Heston model and hence a less good fit of the observed option prices (at least in our implementation with the SSVI forward variance curve). Secondly, the rBergomi does not provide realistic variance sample paths in the long run due to the huge level of the vol-of-var parameter and an exponentially increasing quantity $\mathbb{V}^{\mathbb{P}^*}[v_u|\mathcal{F}_t]$ (leading to extreme values for large u). Furthermore, this model is fairly slow in terms of running time, which appears problematic for calibration and option pricing. To quote El Euch et al. [19]: *"Even with the introduction of the efficient hybrid scheme* [of Bennedsen et al. [8]], *practical implementation* [*of the rBergomi model*] *has proved to be difficult."* One solution to improve the stability and efficiency of this pricing model is to use asymptotics such as in Fukasawa [23], in Forde and Zhang [22] or in Bayer et al. [5]. Finally, Bayer et al. [6] propose a neural network approach to calibrate more accurately the rBergomi and to approximate the implied volatility surface. We will however not deepen these methods in this paper.

8 Life insurance contract valuation

Although all models are well calibrated and hence vanilla options have approximately the same prices under all models, exotic option prices can differ dramatically. It is important to point out that vanilla options determine the marginal distribution (at maturity T of the option), not the process. Indeed, the underlying fine-grain properties of the process have an important impact on path-dependent option prices. We

now highlight the impact of exotic price ranges between our four calibrated models by valuating our endowment life insurance contract described in Sect. 2. This way, we also emphasize the impact of rough volatility models on long-term insurance contracts and compare more thoroughly the rBergomi model (5) and the rough Heston model (8) in terms of long-term properties. For further reference on equity-linked endowment valuation, we refer to Bacinello et al. [3].

8.1 Valuation

By the first fundamental theorem of asset pricing, the fair value at time $t = 0$ of the cash-flow F_t in (1) is given by its discounted expected value under a risk-neutral measure $\mathbb{P}^*$. However, this cash flow also depends on the path of the Poisson process N_t which is not known at time $t = 0$. Therefore, we take the following expectation conditionally to the filtration $\mathcal{G}_0$ to obtain the fair value of our equity-linked endowment contract

$$FV_0 = \mathbb{E}\left[(1 - N_T)\, e^{-rT}\, \mathbb{E}^{\mathbb{P}^*}[F_T \mid \mathcal{F}_0] + \int_0^T e^{-rt}\, \mathbb{E}^{\mathbb{P}^*}[F_t \mid \mathcal{F}_0]\, dN_t \,\middle|\, \mathcal{G}_0\right].$$

The processes N_t and S_t being independent, we obtain that

$$FV_0 = {}_Tp_x\, e^{-rT}\, \mathbb{E}^{\mathbb{P}^*}[F_T] + \int_0^T e^{-rt}\, \mathbb{E}^{\mathbb{P}^*}[F_t]\, {}_tp_x\, \mu_x(t)\, dt\,.$$

We now want to price this insurance contract with the four models we calibrated above (Heston, Bates, rBergomi and rough Heston). We can then use a Monte-Carlo approach to simulate their price process S_t (and variance process v_t) and take the average of the paid benefit under each simulation $j = 1, ... m$ in order to derive the expectation under $\mathbb{P}^*$, i. e.:

$$FV_0 = \frac{1}{m} \sum_{j=1}^{m} \left(e^{-rt_n} F_{t_n j}\, \mathbb{1}\left\{\sum_{i=0}^{n} \Delta N_{t_i, j} = 0\right\} + \sum_{i=0}^{n} e^{-rt_i} \Delta N_{t_i, j}\, F_{t_i, j}\, \mathbb{1}\left\{\sum_{k=0}^{i-1} \Delta N_{t_k, j} = 0\right\}\right),$$

where the underlying price process in F_t is defined by the risk-neutral pricing equation of each model. The discretization of their price process and variance process is given in the previous Sect. 6. Moreover, the use of a Poisson process above makes it easy to add the mortality effect in the simulations to compute FV_0. Indeed, for each simulation $j \in m$, we generate $n = T/\Delta t = 5/0.001 = 5000$ Poisson random variables $\Delta N_{t_i, j}$ with parameter $\lambda = \mu_x(t_i)\, \Delta t$ for $i = 0, ..., n$. For the first i where $\Delta N_{t_i, j} = 1$, we compute a death benefit $F_{t_i, j}$ and if $\Delta N_{t_i, j} = 0$ for all i, we compute a survival benefit $F_{t_n j}$.

We consider the following contracts:

- A female policyholder aged $x = 50$ or $x = 65$ at time $t = 0$.
- We use the Belgian regulatory life table FR for the Makeham force of mortality $\mu_x(t)$.

Table 1 Parameters of the equity-linked endowments

N of contract	Gender	Initial age	κ_g	κ_m	π	Maturity T
1)	Female	50	0.01	0.2	0.8	5
2)	Female	50	0.01	0.2	0.8	10
3)	Female	50	0.01	0.2	0.4	10
4)	Female	50	0.01	0.4	0.8	10
5)	Female	65	0.01	0.2	0.8	15

Table 2 Fair value of the endowment contracts with $\xi_0^{SSVI}(t)$

N of contract	Heston	Bates	rBergomi	Rough Heston
1)	14 017.18 €	13 442.93 €	12 365, 27 €	12 363.09 €
2)	19 353.14 €	17 649.19 €	14 893.48 €	14 130.58 €
3)	14 980.08 €	14 291.13 €	12 916.11 €	12 755.05 €
4)	20 853.01 €	19 079.05 €	15 412.74 €	15 070.89 €
5)	24 909.56 €	21 770.53 €	16 846.11 €	15 425.45 €

Table 3 Fair value of the endowment contracts with $\xi_0^{cst}(t)$

N of contract	Heston	Bates	rBergomi	Rough Heston
1)	14 017.18 €	13 442.93 €	12 527.35 €	12 836.3 €
2)	19 353.14 €	17 649.19 €	15 499.17 €	15 430.33 €
3)	14 980.08 €	14 291.13 €	13 261.24 €	13 386.86 €
4)	20 853.01 €	19 079.05 €	16 294.61 €	16 762.31 €
5)	24 909.56 €	21 770.53 €	17 925.66 €	17 513.7 €

– The initial amount F_0 invested in the fund equals 10 000 €.
– The policyholder pays a unique premium P at time $t = 0$. Note that we could have imposed in the following that $FV_0 = P = F_0 = 10\,000$ € so as to make the contract *fair* and then determine the corresponding κ_g, κ_m or π in (1) that verifies this condition. However, since we aim to compare the contract's value FV_0 between models, we prefer to fix arbitrary values for κ_g, κ_m and π and then derive the corresponding value of the contract.
– We then assume the parameters in Table 1 when valuating the contract.

We obtain in Table 2 the fair values of the endowments with our different models[4] using Monte-Carlo simulations with $m = 200\,000$ and working with the SSVI forward variance curve $\xi_0^{SSVI}(t)$ for the rBergomi and rough Heston models:

---

[4] Note that we consider here the standard version of the Heston model. Similar results are given in Appendix with the forward-variance specification of the Heston model.

We can compare Table 2 with the following Table 3 computed using the constant forward variance curve $\xi_0^{cst}(t) = 0.0925$.

We first see that the Heston model leads to a higher price than the Bates model in both tables. Indeed, even if the long-term variance is higher in the Bates model, the negative average jumps combined with a lower initial variance v_0 and a lower speed of mean reversion λ lead to a lower price in the Bates model. Secondly, we have that rough-type models have a lower price than standard SV models. This can be partly explained in Table 2 by the long-term variance (equal on average in rough models to $\xi_0^{SSVI}(t)$), which is lower than the long-term mean θ^* in the Heston and Bates model as depicted on Fig. 5. However, if we analyze Table 3, we still have lower prices for rough volatility models even if the average long-term variance is this time comparable. This remaining difference can thus be explained by the very long reversion time scale in rough volatility models ($\lambda \rightarrow 0$) and by the rough properties of the variance process (i.e. the parameter H). Moreover, we can see that the rBergomi model tends to have a higher fair value than the rough Heston due to its lower Hurst index H and the extreme values of $\mathbb{V}^{\mathbb{P}^*}[v_u|\mathcal{F}_t]$ when u is large. This is especially true at long time scales and when the participation rate π is high. Finally, comparing the different contracts, we clearly see that the larger the maturity, the higher is the difference between rough volatility models and standard SV models. This will be confirmed with Table 5 below. Moreover, when the participation rate π decreases, the fair value of the contract is logically lower since the policyholder earn a lower portion of the yearly returns. This lower π also lead to less pronounced differences between rough and standard SV models since their divergent sample paths properties play a lesser role. We observe the same effect when the maximal yearly return κ_m increases, with higher differences in fair value between rough and standard SV models due to their divergent sample paths.

Since we said that the rough Heston model is the most consistent with risk-neutral data while enjoying the best long-term properties, we retain the fourth column of Table 2 as being the contracts' prices which are the most market-consistent. We confirm these effects with the two following tables, displaying the fair value FV_0 in function of the minimum yearly guaranteed rate k_g and the maturity of the contract T. These two tables are computed using the SSVI forward variance curve but similar tables derived from $\xi_0^{cst}(t)$ and from $\xi_0^{mkt}(t)$ can be found in Appendix with Tables 6 and 7 and 8 and 9, respectively. These tables in Appendix are also consistent with the following analyses.

We observe the highest differences between rough and standard SV models when k_g tends to be small. Indeed, in this case, the minimum yearly guarantee is exercised less often and therefore the yearly returns, which are highly influenced by the sample paths, play a more important role. This thus leads to stronger differences in fair value between models with divergent sample path properties.

The differences in fair value between models are also the most exacerbated when the maturity of the contract is large. The impact of the sample paths properties of each model is indeed stronger at longer time scales. In particular, the differences in long-term behavior of the variance process are exacerbated when the maturity is large, as explained in the previous sections and in Appendix. Combined with the fact that rough volatility models better reproduce the statistical properties of the

historical volatility thanks to their memory properties, this confirms the importance and the added value of using rough volatility models at large time scales (and especially the rough Heston). Particularly, the importance of the Hurst index (controlling the roughness and memory of the variance process) is emphasized in Appendix when comparing the fair values obtained with the different forward variance curves and with the forward-variance specification of the Heston model. We indeed show that this Hurst index has a huge impact on the contracts' fair values, especially for large maturities. We finally want to highlight that the numbers given in the tables above can slightly change for each run of simulations but are quite stable with our chosen m, equal to 200 000.

9 Conclusion

Rough fractional stochastic volatility models are excellent candidates for reproducing important stylized facts of the past volatility time series and for providing a consistent implied volatility surface with the observed one. In this paper, we explore more closely two tractable implementations of the RFSV model, the rBergomi and the rough Heston models. We show how to expand these two rough volatility models at larger time scales, we analyze their implications for the pricing of long-term life insurance claims and we explain why they provide a more accurate fair value of such long-term contracts. In particular, we study the long-term properties of these two rough volatility models and compare them with two standard SV models (the Heston and Bates models).

Among these four models, we conclude that the rough Heston is the most consistent with historical and risk-neutral data while enjoying the best long-term properties. Indeed, this rough Heston model with $H \approx 0.15$ tends to outperform standard SV models in terms of calibration with a better fit of the implied volatility surface and allows to better reproduce the statistical properties of the observed historical volatility, especially at long time scales. We also retain the rough Heston model as a highly tractable implementation of rough volatility models with only three parameters to estimate and a characteristic function available in quasi-closed form, which is not the case of the rBergomi model. Combined with the Carr-Madan formula, the calibration and pricing of European options with the rough Heston model is hence extremely fast and accurate. Moreover, we manage to build at large time scales a stable regime for the variance process in the rough Heston based on a SSVI parametrization of the forward variance curve. This way, we obtain a model with a reasonable long-term behavior for its variance process while being consistent with the absence of static arbitrage. This rough Heston is thus able to overcome the extreme and exponentially increasing variability of the rBergomi variance process. Using the pricing methodology introduced in this paper, a more accurate fair value of long-term equity-linked life insurance contracts is then obtained in comparison with the rBergomi and standard SV models. This is especially true at large maturity where the good properties of the rough Heston model have a stronger impact. More precisely, we obtain with the rough Heston model a fair value significantly lower than

in standard SV models due to the long-reversion time scale and the rough property of volatility. This highlights the added-value of using this rough Heston model when pricing long-term life insurance contracts.

As future work, we should re-calibrate all the models considered in this paper on other market data of European options. Choosing an other index/stock with a larger set of available maturities and at another point in time should help us to confirm and validate the results derived with our methodology. Moreover, more advanced mortality models could be considered such as in [29] or in [11].

Appendix

SSVI forward variance curve

The surface SVI (SSVI) introduced in [25] provides a tractable arbitrage-free parametrization of the implied volatility surface. SSVI is based on a simple closed-form representation of this volatility surface, which allows an extremely efficient calibration of this parametrization to observed implied volatility data. For a more detailed survey on such surface SVI, we refer to [25]. We simply recall here that SSVI parametrizes the total implied variance (usually denoted $w(k, \theta_t)$) in terms of the log-strike k, of the ATM total variance θ_t (which is assumed to be read on the market), of a constant leverage parameter ρ and of a curvature function $\varphi(\theta_t)$. We will consider the widely-used power-law curve for φ,

$$\varphi(\theta_t) = \frac{\eta}{\theta_t^{\gamma} \left(1 + \theta_t\right)^{1-\gamma}},$$

since it allows a SSVI volatility surface completely free of static arbitrage (no calendar spread and butterfly arbitrages) provided that $\gamma \in (0, 1/2)$ and $\eta(1 + |\rho|) \leq 2$. This function also allows to be consistent with the power-law shape of the observed term structure of ATM volatility skew (cfr Sect. 5).

We then used the algorithm described in Section 5.2 of [25] with our power-law SSVI in order to calibrate the parameters (ρ, η, γ) to implied volatility data while avoiding static arbitrage. The optimal parameters ρ^*, η^* and γ^* are equal respectively to $(-0.6842, 1.1536, 0.3410)$ in such a way that the non-arbitrage conditions above are verified. With these parameters, we obtain Fig. 12 below depicting the excellent fit of the power-law SSVI parametrization to observed implied volatility data.

We observe that the fit quality is almost perfect. There is only a slight deviation from the data for the shortest maturity $T = 0.027$. The associated forward variance curve to this SSVI parametrization is then given by Fig. 13 and is again obtained as in [24] by approximating the value of a variance swap by the value of a log-contract of the same maturity, built this time upon the SSVI parametrization of the volatility surface. Note that this SSVI forward variance curve is interpolated between observed maturities such as to ensure the absence of arbitrage in the interpolated volatility surface, following the methodology described in Section 5.3 of [25].

The objective now is to extrapolate in an arbitrage-free way the SVI surface beyond the last available maturity $T = 1.2$. As explained again in Section 5.3 of [25], we first need a monotonic increasing extrapolation of θ_t which is asymptotically linear in time. Based on Fig. 14 below depicting the values of θ_t for the observed maturities, we clearly see that a simple linear regression appears to provide the best fit (while being of course asymptotically linear in time).

Let t_n be the last available maturity in the data. According to [25], the total implied variance for $t > t_n$ can now be extrapolated by

$$w(k, \theta_t) = w(k, \theta_{t_n}) + \theta_t - \theta_{t_n},$$

while remaining free of static arbitrage (cfr Theorem 4.3 [25]). Finally, the forward variance curve is again retrieved from the extrapolated values $w(k, \theta_t)$ by valuating log-contracts. The extrapolated forward variance curve based on this power-law SSVI parametrization is depicted in Sect. 4.3 on Fig. 5.

Calibration and valuation based on other forward variance curves

Constant forward variance curve

Rough Heston

Using the constant forward variance curve $\xi_0^{cst}(t) = 0.0925$, we obtain in a first step the following set of initial parameters from the SA global optimizer: (0.1235, 0.6383, −0.6415). Using our local optimizer, we then find a minimal RMSE of 0.11097 with the following (same) final parameter values Θ^*:

H^*	ν^*	ρ^*
0.1235	0.6383	− 0.6415

The fit is thus poorer than with the initial SSVI forward variance curve $\xi_0^{SSVI}(t)$. The vol-of-var parameter ν^* and the anti-correlation ρ^* are close to values obtained previously with $\xi_0^{SSVI}(t)$ but the Hurst index H^* is now lower and closer to the historical estimate ($= 0.13$).

rBergomi

Using $\xi_0^{cst}(t) = 0.0925$, we find a RMSE of 0.0851 with the initial set of parameters (0.12, 1.55, −0.90). This leads to the following final parameter values Θ^*:

H^*	η^*	ρ^*
0.1231	1.8636	− 0.8951

Hence, we obtain a slightly better fit than with the rBergomi based on the SSVI forward variance curve (and almost as good as the SSVI Rough Heston). However, we have an even higher vol-of-var parameter compared with the SSVI forward variance curve

Table 4 Fair value FV_0 for various k_g with maturity $T = 10$ and with $\xi_0^{SSVI}(t)$

$T = 10$	Heston	Bates	rBergomi	Rough Heston
$k_g = 0.5\%$	18 931.16 €	17 255.14 €	14 494.43 €	13 696.86 €
$k_g = 1\%$	19 353.14 €	17 649.19 €	14 893.48 €	14 130.58 €
$k_g = 2\%$	20 262.77 €	18 498.54 €	15 795.31 €	15 130.80 €
$k_g = 5\%$	23 644.91 €	21 649.22 €	19 418.47 €	19 072.87 €

Table 5 Fair value FV_0 for various maturities T with $k_g = 1\%$ and with $\xi_0^{SSVI}(t)$

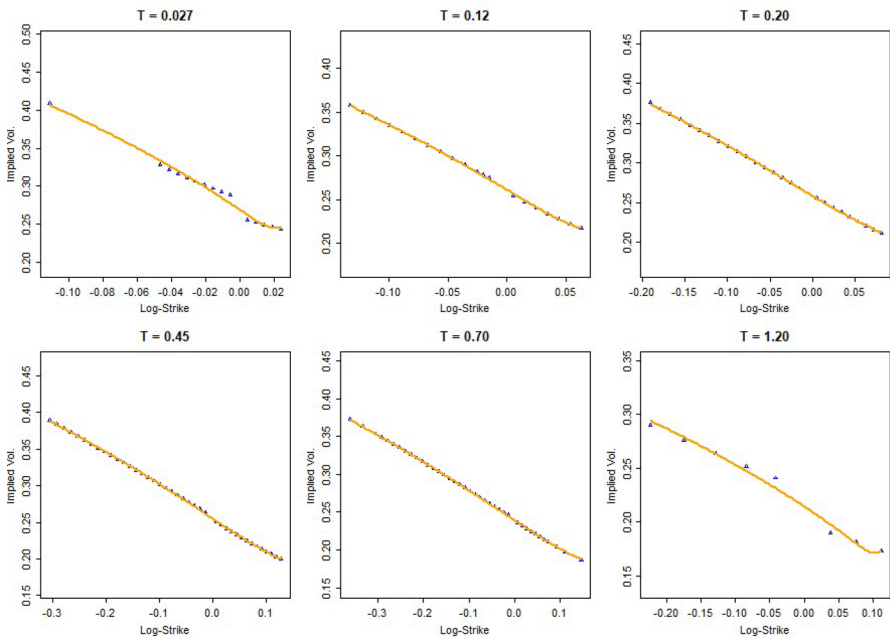| $k_g = 1\%$	Heston	Bates	rBergomi	Rough Heston
$T = 5$	14 017.18 €	13 442.93 €	12 365.27 €	12 363.09 €
$T = 10$	19 353.14 €	17 649.19 €	14 893.48 €	14 130.58 €
$T = 20$	35 618.91 €	29 613.34 €	20 126.21 €	17 677.04 €

Fig. 12 Blue dots are the observed mid implied volatilities, the orange solid line is the power-law SSVI fit

$$v^* = \eta^* \sqrt{2H^*}/(2\,C_H) = 1.137$$

This huge level v^* again leads to unrealistic sample paths. We also obtain a lower Hurst index H^*. Moreover, we still have a stability issue when calibrating this rBergomi model with a high variability of the results in function of the chosen number of paths and steps (here, $m = 1\,000\,000$ and $n = 300$ for the calibration).
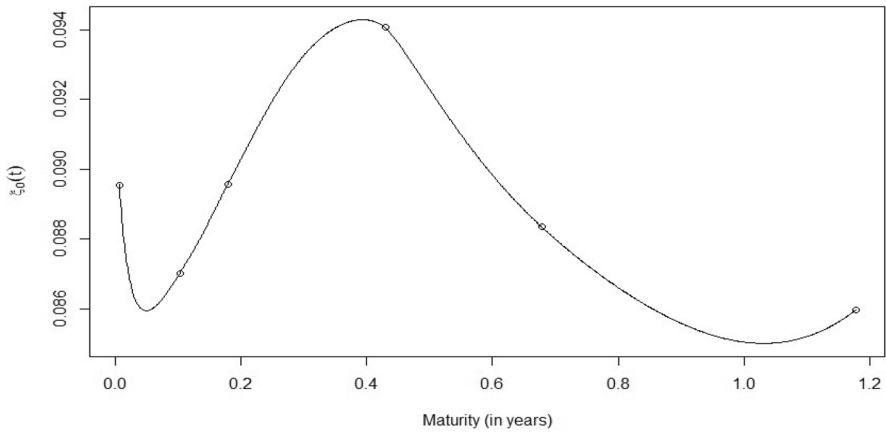
Fig. 13 Initial SSVI forward variance curve $\xi_0^{SSVI}(t)$ between 0 and 1.2 years. The black dots are the values of $\xi_0^{SSVI}(t)$ for the observed maturities
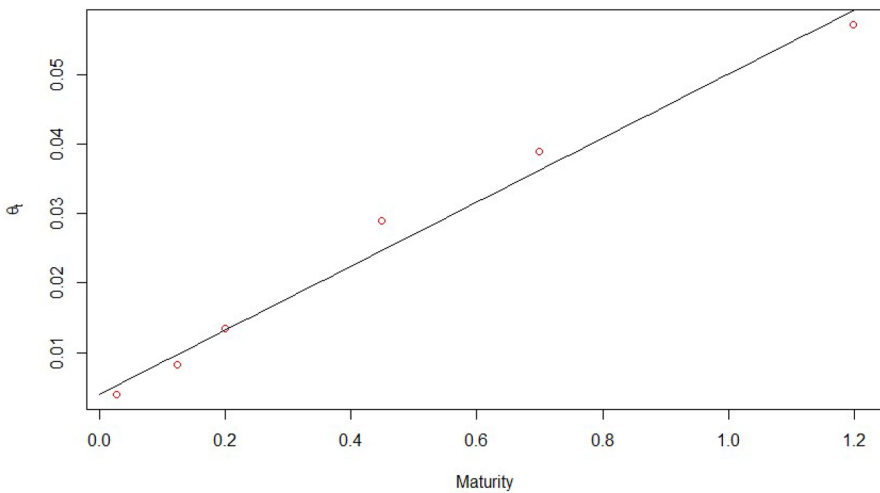

Fig. 14 Red dots are values of θ_t for the available maturities, the red line is the linear fit

Table 6 FV_0 for various k_g with maturity $T = 10$ and $\xi_0^{cst}(t)$

$T = 10$	rBergomi	Rough Heston
$k_g = 0.5\%$	15 086.55 €	15 041.99 €
$k_g = 1\%$	15 492.96 €	15 430.33 €
$k_g = 2\%$	16 403.19 €	16 334.91 €
$k_g = 5\%$	20 015.25 €	20 048.91 €

Furthermore, the two Tables 6 and 7 display the fair value FV_0 in function of the minimum yearly guaranteed rate k_g and the maturity of the contract T.

$k_g = 1\%$	rBergomi	Rough Heston
$T = 5$	12 527.35 €	12 836.30 €
$T = 10$	15 492.96 €	15 430.33 €
$T = 20$	22 079.51 €	21 124.48 €

Table 7 FV_0 for various maturities T with $k_g = 1\%$ and $\xi_0^{cst}(t)$

If we compare these two tables with Tables 4 and 5 derived from the SSVI forward variance curve, we see that the obtained fair values are significantly higher when using the constant forward variance curve $\xi_0^{cst}(t)$. For the rough Heston, we said above that the main difference in terms of calibration is the lower Hurst index when considering $\xi_0^{cst}(t)$. Therefore, the comparison of these two forward variance curves shows the impact of the roughness and memory properties of the variance process on the contracts' prices. A lower Hurst index leads to a higher fair value. Moreover, we observe that the differences in fair values when considering the two forward variance curves are the most exacerbated at large time scales. This comparison hence emphasizes the importance of taking the roughness/memory property of the variance process into account, especially for large maturities.

Market forward variance curve

Rough Heston

Using the market forward variance curve $\xi_0^{mkt}(t)$, we obtain in a first step the following set of initial parameters from the SA global optimizer: (0.1206, 0.4131, − 0.8015). We then obtain with our local optimizer a minimal RMSE of 0.09235 with the following (same) final parameter values Θ^*:

H^*	v^*	ρ^*
0.1206	0.4131	− 0.8015

The fit is thus poorer compared with the fit derived from the SSVI forward variance curve but better than when using $\xi_0^{cst}(t)$. The Hurst index is again lower and very close to the historical estimate. We also observe that the volatility of variance parameter v^* is lower compared to the SSVI parametrization and we obtain this time a stronger anti-correlation ρ^*.

rBergomi

We find a RMSE of 0.1479 with the initial set of parameters equal to (0.1, 1.45, − 0.99). This leads to the following final values Θ^*:

H^*	η^*	ρ^*
0.1357	1.4614	− 0.9967

The quality of the fit is clearly poorer compared with $\xi_0^{SSVI}(t)$ and $\xi_0^{cst}(t)$. The vol of var parameter is this time lower and more reasonable. We indeed have

Table 8 Fair value FV_0 for various k_g with maturity $T = 10$ and $\xi_0^{mkt}(t)$

$T = 10$	rBergomi	Rough Heston
$k_g = 0.5\%$	14 518.48 €	13 817.37 €
$k_g = 1\%$	14 909.54 €	14 228.54 €
$k_g = 2\%$	15 785.42 €	15 196.15 €
$k_g = 5\%$	19 301.23 €	19 075.75 €

Table 9 Fair value FV_0 for various maturities T with $k_g = 1\%$ and $\xi_0^{mkt}(t)$

$k_g = 1\%$ s	rBergomi	Rough Heston
$T = 5$	12 291.17 €	12 371, 10 €
$T = 10$	14 909.54 €	14 228.54 €
$T = 20$	20 639.81 €	18 293.85 €

$v^* = \eta^* \sqrt{2 H^*}/(2 C_H) = 0.8804$. We again obtain a lower Hurst index compared with the SSVI forward variance curve.

Since the market forward variance curve lies below the SSVI forward variance curve for the considered maturities, we would expect a lower fair value of our contract using $\xi_0^{mkt}(t)$ instead of $\xi_0^{SSVI}(t)$. However, for both the Rough Heston and the rBergomi, the lower Hurst index H and the lower parameter v both lead to an increase of the contract's prices and hence, they compensate for the lower average values of v_t. This is why we observe very similar fair values when using the two forward variance curves (cfr Tables 8 and 9 vs. Tables 4 and 5). For large maturities or small values of κ_g, we see that we even obtain a higher fair value when using the market forward variance curve $\xi_0^{mkt}(t)$. Again, this comes from the fact that the sample paths properties are exacerbated when the maturity is large or when the minimal guarantee κ_g is low. This comparison also shows that the Hurst index H (and hence the roughness/memory property of the variance process) has a strong impact on the fair value of insurance contracts, especially at large time scales. This emphasizes once again the importance of using rough volatility models.

Forward Heston model

In order to provide a better comparison with rough volatility models, we finally introduce the forward-variance specification of the Heston model. From Gatheral and Keller-Ressel [27], we have that the Heston model is an affine forward variance model, as explained in Sect. 3.2. Hence, the characteristic function of the log-asset price $X_t = \log S_t$ at time 0 under the Heston model can be written as previously by (9) where we use the SSVI forward variance curve $\xi_0^{SSVI}(t)$ and where we need to solve the Riccati ODE (10). Using well-known numerical methods to solve this Riccati ODE and applying the Carr-Madan formula with the characteristic function above, it is quite simple to calibrate and find the optimal parameters (λ^*, ρ^*, v^*)

Table 10 FV_0 for various k_g with maturity $T = 10$ and $\xi_0^{SSVI}(t)$

$T = 10$	Heston	fwd Heston	rBergomi	Rough Heston
$k_g = 0.5\%$	18 931.16 €	17 370.17 €	14 494.43 €	13 696.86 €
$k_g = 1\%$	19 353.14 €	17 750.09 €	14 893.48 €	14 130.58 €
$k_g = 2\%$	20 262.77 €	18 581.37 €	15 795.31 €	15 130.80 €
$k_g = 5\%$	23 644.91 €	21 790.04 €	19 418.47 €	19 072.87 €

Table 11 FV_0 for various maturities T with $k_g = 1\%$ and $\xi_0^{SSVI}(t)$

$k_g = 1\%$	Heston	fwd Heston	rBergomi	Rough Heston
$T = 5$	14 017.18 €	13 442.93 €	12 365.27 €	12 363.09 €
$T = 10$	19 353.14 €	17 750.09 €	14 893.48 €	14 130.58 €
$T = 20$	35 618.91 €	28 928.57 €	20 126.21 €	17 677.04 €

based on the observed European options and based on the SSVI forward variance cure $\xi_0^{SSVI}(t)$. We find a RMSE of 0.1182 with the following optimal parameters:

λ^*	ν^*	ρ^*
3.02522	1.42928	-0.71762

The RMSE and the final parameters of this forward-variance specification of the Heston model are highly similar to the ones derived above in Section 4.2 for the classical Heston model. However, for pricing our life-insurance contract, we still need to calibrate the mean-reversion level θ and the initial variance level v_0. The constant parameter θ is not flexible enough to deal with the observed forward variance curve and we therefore need to consider an extension of the Heston model where we allow the mean-reversion level $\theta(t)$ to be time-dependent. In order to fit the market and recover the SSVI forward variance curve, the authors in [10] show that we must set

$$\theta(t) = \frac{\frac{\partial}{\partial t}\xi_0^{SSVI}(t)}{\lambda} + \xi_0^{SSVI}(t) \quad \text{and} \quad v_0 = \xi_0^{SSVI}(0).$$

This indeed allows to have $\mathbb{E}^{\mathbb{P}^*}[v_t|\mathcal{F}_0] = \xi_0^{SSVI}(t)$ in this model. We then obtain the following Tables 10 and 11 giving the fair value FV_0 of the contracts above under the forward-variance specification of the Heston model.

We clearly see that the forward-variance specification of the Heston model provides lower fair values compared with the standard Heston model due to the lower mean-reversion level. The mean-reversion function $\theta(t)$ indeed lies below the value $\theta^* = 0.0967$ of the standard Heston model at any time scales. We again see that this forward-variance Heston model provides a higher fair value than rough volatility models even if their average long-term variance is this time comparable since $\mathbb{E}^{\mathbb{P}^*}[v_t|\mathcal{F}_0] = \xi_0^{SSVI}(t)$ in each model. This once again emphasizes that the rough property of the variance process induced by the index H^* has a strong impact on the obtained fair values of long-term life insurance contracts.

Table 12 European risk-free interest rates between 0 and 20 years

Maturity	Rate	Maturity	Rate
Overnight	−0.55486 %	8 years	−0.26535 %
7 days	−0.52686 %	9 years	−0.23026 %
1 month	−0.494 %	10 years	−0.19118 %
2 months	−0.44157 %	11 years	−0.15312 %
3 months	−0.43514 %	12 years	−0.11707 %
6 months	−0.35386 %	13 years	−0.08303 %
1 year	−0.36767 %	14 years	−0.07203 %
2 years	−0.38775 %	15 years	−0.02600 %
3 years	−0.39076 %	16 years	−0.00200 %
4 years	−0.37771 %	17 years	0.00099 %
5 years	−0.35563 %	18 years	0.0020 %
6 years	−0.33054 %	19 years	0.01100 %
7 years	−0.29945 %	20 years	0.03599 %

Figures

Risk-free rates

Conditional variance process

The rBergomi variance process is conditionally log-normal and we can prove that

$$\mathbb{V}_{\mathbb{P}^*}[v_u|\mathcal{F}_t] = \xi_t(u)^2 \left(\exp\left(\eta^2(u-t)^{2H}\right) - 1\right). \tag{17}$$

Hence, this quantity increases exponentially with u, leading to extreme swings and variability in the rBergomi variance process for large maturities. We see that $\mathbb{V}_{\mathbb{P}^*}[v_u|\mathcal{F}_t]$ also depends on the forward variance curve, but since this curve is stable for large maturity (cfr Fig. 5 and 4), it does not contribute to the exponential growth of $\mathbb{V}_{\mathbb{P}^*}[v_u|\mathcal{F}_t]$.

For the rough Heston, using Ito isometry and conditional log-normality, we find

$$\mathbb{V}_{\mathbb{P}^*}[v_u|\mathcal{F}_t] = \frac{v^2}{[\Gamma(H+1/2)]^2} \int_t^u (u-s)^{2H-1} \xi_t(s)\, ds. \tag{18}$$

Since the forward variance curve is almost constant for large maturities, we make the assumption that this curve is fixed to a constant K so as to obtain the following approximation at $t = 0$:
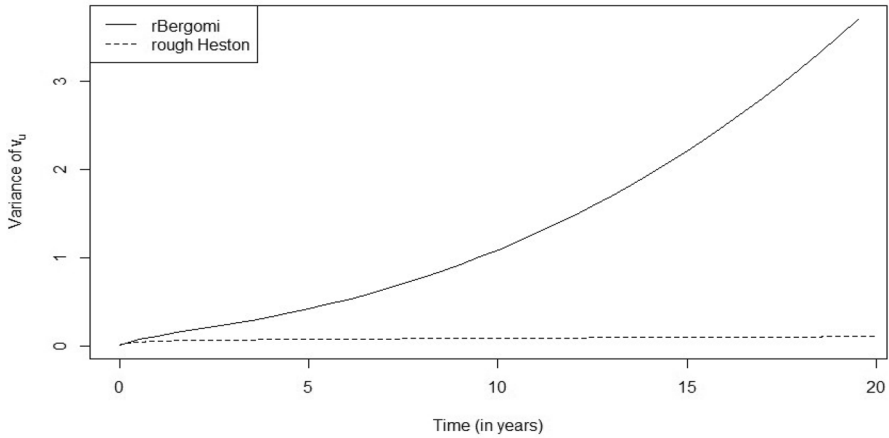
Fig. 15 Comparison of $\mathbb{V}_{\mathbb{P}^*}[v_u|\mathcal{F}_0]$ in function of u between the rough Heston and the rBergomi models

$$\mathbb{V}_{\mathbb{P}^*}[v_u|\mathcal{F}_0] \approx \frac{K\,v^2}{\left[\Gamma(H+1/2)\right]^2 2H}\,u^{2H}\,.$$

This approximation allows to see that the rate of increase of the quantity $\mathbb{V}_{\mathbb{P}^*}[v_u|\mathcal{F}_0]$ is approximately u^{2H}, which leads to a slowly increasing behavior as confirmed on Fig. 15. Using the SSVI forward variance curve $\xi_0^{SSVI}(u)$ in (17) with $\eta = 1.6803$ and $H = 0.1515$ and using again $\xi_0^{SSVI}(u)$ with $v = 0.6241$ and $H = 0.1703$ in equation 18, we obtain the following figure Fig. 15 at $t = 0$.

ATM volatility skew term structure
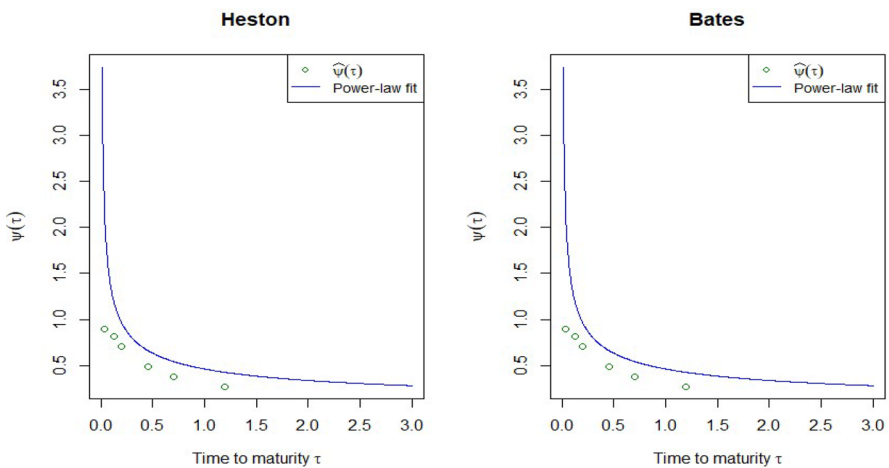
Fig. 16 Empirical fit (blue) vs. Heston and Bates fit (green) of $\psi(\tau)$, CAC 40
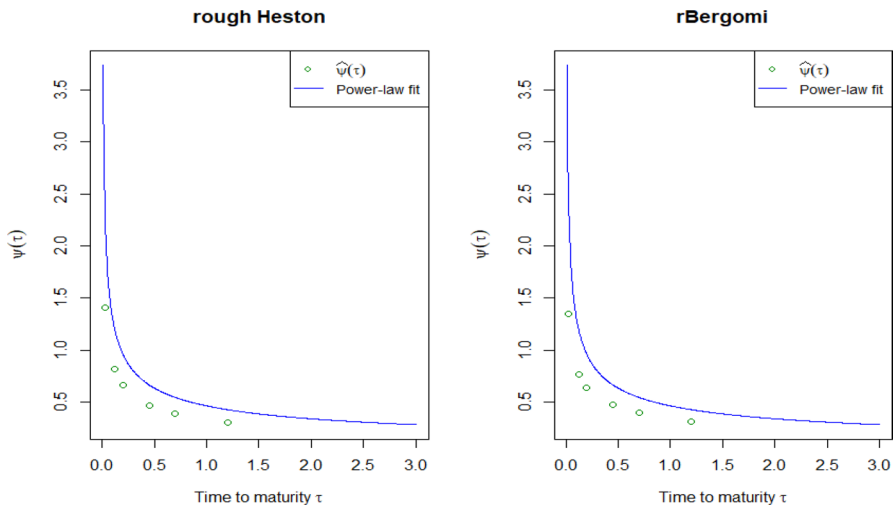
Fig. 17 Empirical fit (blue) vs. rough Heston and rBergomi fit (green) of $\psi(\tau)$, CAC 40

Availability of data and material The datasets and code generated during and/or analyzed during the current study are available from the corresponding author on reasonable request.

Declarations

Conflict of interest The authors declare that they have no conflict of interest.

References

1. Abi Jaber E (2019) Lifting the Heston model. Quant Financ 19(12):1995–2013
2. Abi Jaber E, El Euch O (2019) Multifactor approximation of rough volatility models. SIAM J Financ Math 10(2):309–349
3. Bacinello AR, Biffis E, Millossovich P (2010) Regression-based algorithms for life insurance contracts with surrender guarantees. Quant Financ 10(9):1077–1090
4. Bayer C, Friz P, Gatheral J (2016) Pricing under rough volatility. Quant Financ 16(6):887–904
5. Bayer C, Friz PK, Gulisashvili A, Horvath B, Stemper B (2019a) Short-time near-the-money skew in rough fractional volatility models. Quant Financ **19**(5), 779–798
6. Bayer C, Horvath B, Muguruza A, Stemper B, Tomas M (2019b) On deep calibration of (rough) stochastic volatility models. arXiv:1908.08806
7. Bennedsen M, Lunde A, Pakkanen MS (2016) Decoupling the short-and long-term behavior of stochastic volatility. arXiv:1610.00332
8. Bennedsen M, Lunde A, Pakkanen MS (2017) Hybrid scheme for brownian semistationary processes. Financ Stochast 21(4):931–965
9. Bergomi L, Guyon J (2012) Stochastic volatility's orderly smiles. Risk 25(5):60
10. Buehler H (2006) Consistent variance curve models. Financ Stochast 10(2):178–203
11. Cairns AJ, Blake D, Dowd K (2008) Modelling and management of mortality risk: a review. Scand Actuar J 2008(2–3):79–113

12. Carr P, Madan D (1999) Option valuation using the fast fourier transform. J Comput Financ 2(4):61–73
13. Chen X, Li WV, Rosiński J, Shao QM (2011) Large deviations for local times and intersection local times of fractional brownian motions and Riemann-Liouville processes. Ann Probab 39(2):729–778
14. Cheridito P, Kawaguchi H, Maejima M (2003) Fractional Ornstein-Uhlenbeck processes. Electron J Probab 8
15. Comte F, Renault E (1998) Long memory in continuous-time stochastic volatility models. Math Financ 8(4):291–323
16. Coutin L, Pontier M (2007) Approximation of the fractional brownian sheet via Ornstein-Uhlenbeck sheet. ESAIM: Probab Stat 11:115–146
17. Cui Y, del Bano Rollin S, Germano G (2017) Full and fast calibration of the Heston stochastic volatility model. Eur J Oper Res 263(2):625–638
18. Dupret JL, Hainaut D (2021) Portfolio insurance under rough volatility and Volterra processes. Int J Theor Appl Financ 24(06–07):2150036
19. El Euch O, Gatheral J, Rosenbaum M (2019) Roughening Heston. Risk pp. 84–89
20. El Euch O, Rosenbaum M (2018) Perfect hedging in rough Heston models. Ann Appl Probab 28(6):3813–3856
21. El Euch O, Rosenbaum M (2019) The characteristic function of rough Heston models. Math Financ 29(1):3–38
22. Forde M, Zhang H (2017) Asymptotics for rough stochastic volatility models. SIAM J Financ Math 8(1):114–145
23. Fukasawa M (2017) Short-time at-the-money skew and rough fractional volatility. Quant Financ 17(2):189–198
24. Gatheral J (2011) The volatility surface: a practitioner's guide, vol. 357. Wiley, Amsterdam
25. Gatheral J, Jacquier A (2014) Arbitrage-free svi volatility surfaces. Quant Financ 14(1):59–71
26. Gatheral J, Jaisson T, Rosenbaum M (2014) Volatility is rough. Quant Financ 18(6):933–949
27. Gatheral J, Keller-Ressel M (2019) Affine forward variance models. Financ Stochast 23(3):501–533
28. Gatheral J, Radoičić R (2019) Rational approximation of the rough Heston solution. Int J Theor Appl Financ 22(03):1950010
29. Hainaut D, Devolder P (2008) Mortality modelling with Lévy processes. Insur Math Econ 42(1):409–418
30. Karatzas I, Shreve SE (1998) Brownian motion. In: Brownian Motion and Stochastic Calculus, pp 47–127. Springer
31. Lord R, Koekkoek R, Dijk DV (2010) A comparison of biased simulation schemes for stochastic volatility models. Quant Financ 10(2):177–194
32. Mandelbrot BB, Van Ness JW (1968) Fractional brownian motions, fractional noises and applications. SIAM Rev 10(4):422–437
33. McCrickerd R, Pakkanen MS (2018) Turbocharging Monte Carlo pricing for the rough Bergomi model. Quant Financ 18(11):1877–1886
34. Moyaert T, Petitjean M (2011) The performance of popular stochastic volatility option pricing models during the subprime crisis. Appl Financ Econ 21(14):1059–1068
35. Mrázek M, Pospíšil J, Sobotka T (2016) On calibration of stochastic and fractional stochastic volatility models. Eur J Oper Res 254(3):1036–1046
36. Ninomiya S, Victoir N (2008) Weak approximation of stochastic differential equations and application to derivative pricing. Appl Math Financ 15(2):107–121
37. Van Laarhoven PJ, Aarts EH (1987) Simulated annealing. In: Simulated annealing: theory and applications, pp 7–15, Springer, New York

Authors and Affiliations

Jean-Loup Dupret[1] ⓘ · **Jérôme Barbarin**[1] · **Donatien Hainaut**[1]

Jérôme Barbarin
jerome.barbarin@uclouvain.be

Donatien Hainaut
donatien.hainaut@uclouvain.be

[1]   LIDAM, Institute of Statistics, Biostatistics and Actuarial Sciences, Université Catholique de
        Louvain, Louvain-La-Neuve, Belgium